creative commons
COMMONS DEED

저작자표시-비영리-변경금지 2.0 대한민국

이용자는 아래의 조건을 따르는 경우에 한하여 자유롭게

- 이 저작물을 복제, 배포, 전송, 전시, 공연 및 방송할 수 있습니다.

다음과 같은 조건을 따라야 합니다:

저작자표시. 귀하는 원저작자를 표시하여야 합니다.

비영리. 귀하는 이 저작물을 영리 목적으로 이용할 수 없습니다.

변경금지. 귀하는 이 저작물을 개작, 변형 또는 가공할 수 없습니다.

- 귀하는, 이 저작물의 재이용이나 배포의 경우, 이 저작물에 적용된 이용허락조건을 명확하게 나타내어야 합니다.
- 저작권자로부터 별도의 허가를 받으면 이러한 조건들은 적용되지 않습니다.

저작권법에 따른 이용자의 권리는 위의 내용에 의하여 영향을 받지 않습니다.

이것은 이용허락규약(Legal Code)을 이해하기 쉽게 요약한 것입니다.

Disclaimer

dCollection

공학박사 학위논문

Analysis of Dynamic Behavior of Metal Nano-particles with Different Conductivity of Substrate using In-situ TEM : The Effect of Charge

In-situ TEM을 이용한 기판의 전도성에 따른
금속 입 거동의 동역학적 분석 : 하전 효과

2018년 2월

서울대학교 대학원
재 료 공 학 부
김 근 수

Abstract

'Non-classical crystallization' is a remarkable phenomenon in the nanostructure fabrication, which suggests that nanoparticle is the smallest unit as building block in crystal growth. In-situ transmission electron microscopy (in-situ TEM) provides crucial clues in understanding its mechanism. However, many mechanisms still remain unclear, especially the lack of understanding the charge effect caused by inelastic collision of the electron beam with sample in TEM. Here, we report that the structural instability and coalescence are promoted by charging through real-time observation of Au particles on substrates with difference conductivity. From a kinetic point view, this difference implies that the charge enhanced diffusion. This investigation broadens current knowledge of 'non-classical crystallization' that grows by nanoparticles, sheds light on a potential factor to control the nanostructure fabrication. In this thesis, I carefully pay attention to the charge effect caused by the interaction between injected electron beam with high energy and sample during real-time TEM observation. In order to clarify the effect of charging in TEM, first, we clearly reproduced the difference in structure stability of a nanoparticle according to the substrate conductivity.

Furthermore, the coalescence of multi-particles according to the degree of activation by charge was confirmed from the viewpoint of dynamics. Finally,

we attempted to exclude various interpretations occurring within in-situ TEM by constructing a well-established artificial charging system

---

Key words : Non-classical Crystallization, Charged Nanoparticle, Metal Nanoparticle(Gold, Silver), Substrate Conductivity, In-situ Transmission Electron Microscopy (TEM), Floating and Ground system

Student number : 2012-30916

Kunsu Kim

Contents

List of Figures

List of Tables

Ch. 1 Introduction

Nanostructures are small objects in the 10^{-9} meter range, but it has been studied in a variety of fields because it has extraordinary physical and chemical properties caused by high surface-to-volume ratio as well as it can form complex structures depending on the environment and functionality desired. For this reason, a novel field of material science, chemistry and physics that emphasizes the synthesis and control of nanomaterials has emerged for the past decades. What is noteworthy this new nanoworld is that the new characteristics change with size and shape. Thus, how to tailor and control the shape and size of nanostructures and where to apply them is an important issue in nanotechnology.

In the ranging from 0 D (quantum dot) to 3 D structures (complex structure like hierarchical structure) their growth mechanisms are known as diffusion-controlled growth by atom-by-atom (ions / molecules) attachment process. Recently, some novel nanostructures like meso-crystal are hard to describe the mechanism in these classical approach. These phenomenon is comprehended as 'Non-classical crystallization' indicated that the nanostructures are made nanoparticles. Therefore, the study of the behavior of one or multi-particles in the nanometer size regime is so importance for understating the architecture of nanoparticles.

Many studies have reported various mechanisms to explain this phenomenon, but there are still unclear what factors are dominant. Prof.

Hwang suggested a new approach of this phenomenon as the effect of charge, but this theory was not accepted by the barriers of well-established growth theories due to the limitations of indirect experimental evidence.

This thesis experimentally examined the possibility that the charge can be an important factor in non-classical crystallization through direct observation using TEM. Chapter 1 describes the classical versus non-classical growth mechanism, the effects of charge in the growth system, and the charging phenomenon within the transmission electron microscope (TEM)

1.1 Non-classical Crystallization

The nanostructures are synthesized and grown by injecting the target material directly into a sources like solute and reactive gases. This growth must be in a 'supersaturation' condition with sufficient concentration to react. The core of classical crystallization is 'Nucleation and growth', which can be easily understood as a homo-nucleation phenomenon occurring in a solution.

Addition of excess solute to a solvent having solubility for a target solute results in precipitation and formation of nanostructures. Thus, the method for forming the supersaturation can be done by dissolving the solute at high temperature and then lowering it to a low temperature or supplying additional solute to form a supersaturated state. (Eq. 1)

$$\Delta G_v = -\frac{\mathrm{kT}}{\Omega}\ln\left(\frac{C}{C_0}\right) \qquad \text{(Eq. 1)}$$

C : solute concentration, C_0 : equilibrium concentration or solubility, Ω : Atomic volume

The precipitation process then basically consists of a nucleation step followed by particle growth stages. The classical crystallization growth model starts from primary building blocks like atoms, ions or molecules, forming clusters depending on the counter play of surface and crystal lattice energies. Eventually, some clusters reach the size of a so-called critical crystal nucleus. At this stage, the free enthalpy of the system becomes negative upon further particle growth, because the gain in lattice energy overcompensates the loss in surface energy. (Fig. 1, Eq. 2) These primary nanoparticles grow further via atom-by-ion attachment and unit cell replication.

$$\Delta G_{total} = \frac{4\pi r^3}{3}\Delta G_V + 4\pi r^2\gamma \qquad \text{(Eq. 2)}$$

ΔG_{total} : Total free-energy change, r : Radius of nucleus, ΔG_V : volume free energy change, γ : specific surface free energy (or surface energy)

From figure 1, the newly generated nucleus is stable when its radius exceeds a critical size, r^*. A nucleus smaller than r^* will melt and dissolve to reduce the overall free energy, whereas those larger than r^* become stable

and continues to grow. At the critical size $r = r^*$, $\mathrm{d}\Delta\mathrm{G}/\mathrm{dr} = 0$ and critical size, r^*, and critical energy, ΔG^*, are defined by :

$$r^* = -2\gamma/\Delta G_v \quad \text{(Eq. 3)}$$

$$\Delta G^* = 16\pi\gamma/3(\Delta G_v)^2 \quad \text{(Eq. 4)}$$

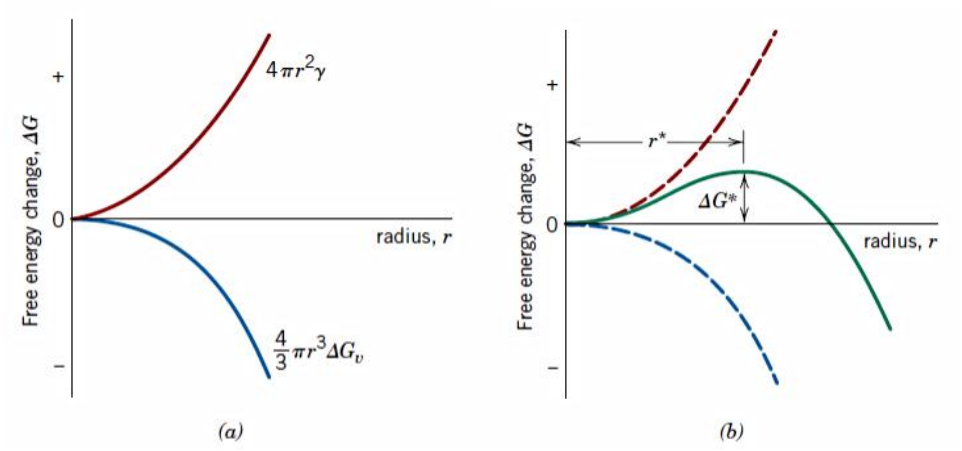

Figure 1 Schematic curves for volume free energy and surface free energy contributions to the total free energy change of a spherical nucleus (b) Schematic plot of free energy versus nucleus radius. ($\boldsymbol{r}^*$: critical nucleus radius, $\Delta\boldsymbol{G}^*$: critical gibbs free energy change)

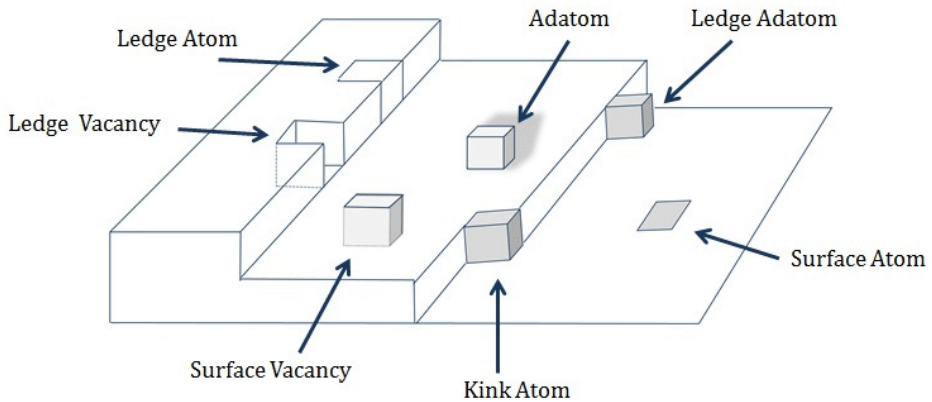

Figure 2 Terrace-Ledge-Kink model, which represents the growth by atom-by-atom attachment.

In this method of atom unit growth, the determination of the incorporation of one atom depends on the surface state of the cluster that becomes critical size.(*1*) When atoms attach to the surface and generate excess energy, these atoms are not incorporated and eventually annihilated, and if they do not give excess energy to the total system, they are incorporated and grow as a whole. This is the basic concept of the TLK model, which is accepted as the main mechanism for the growth of nanostructures such as particles and thin films. (*2*) (Fig. 2) More specifically, when the adatom sits on a terrace on a surface with a smooth interface, it diffuses through the ledge and finally enters the crystal from the kink. Although the shape of inorganic crystals is often related to the intrinsic unit

cell structure, the same material can exhibit diverse crystal morphologies. This behavior is on the one hand due to different surface energies of the crystal faces, and on the other hand due to the external growth environment, i.e., the growth rate of a crystal face is a direct consequence of its surface energy, if the same growth mechanism applies. Crystal faces with high surface energies exhibit the fastest growth rate and are minimized or even disappear in the final morphology. (Fig. 3 (a))

For the past decade, however, many studies have been conducted on 'Non-classical crystallization' phenomenon that nanoparticles act as a building block to form nanostructures. (*3-9*) This concept is new paradigm, which is the different from the classical comprehensions of crystal growth. The non-classical crystallization and growth are nanoparticle mediated and involve a mesoscopic transformation process. (*10*) There are two pathways to form a nanocrystal through the non-classical crystallization. At figure 3 (b), a well aligned or iso-oriented crystal grow by nanoparticles, which can form a single crystal upon fusion of the nanoparticles. If the nanoparticles are coated by some organic ligands or other components, these nanoparticles can form a mesocrystal via nanoparticles assembly. (Fig. 3 (c)) One feature of this mesocrystal formation is the oriented attachment of nanoparticles. Oriented attachment involves self-organization of adjacent particles so that they share a common crystallographic information, followed by joining of these particles. Bonding between the particles reduces total gibbs free energy by removing surface energy associated with

broken bonds. This mechanism is relevant in cases where particles are free to move (such as in solution or where particles have abundant surface-bound water) and probably occurs in nature. It may also apply when particles nucleate side-by-side on a substrate and coalescence during growth. (*11, 12*)

Therefore, the describe the statement of mesocrystal have an important role in understanding the mechanism of non-classical crystallization. However, when the kinetics follows the path of Fig. 3 (b), it would be difficult to distinguish from a final morphology of the crystal whether it grows by an individual atom or nanoparticle. That is the reason why the crystal growth by nanoparticles had a great resistance in the crystal growth community in early years.

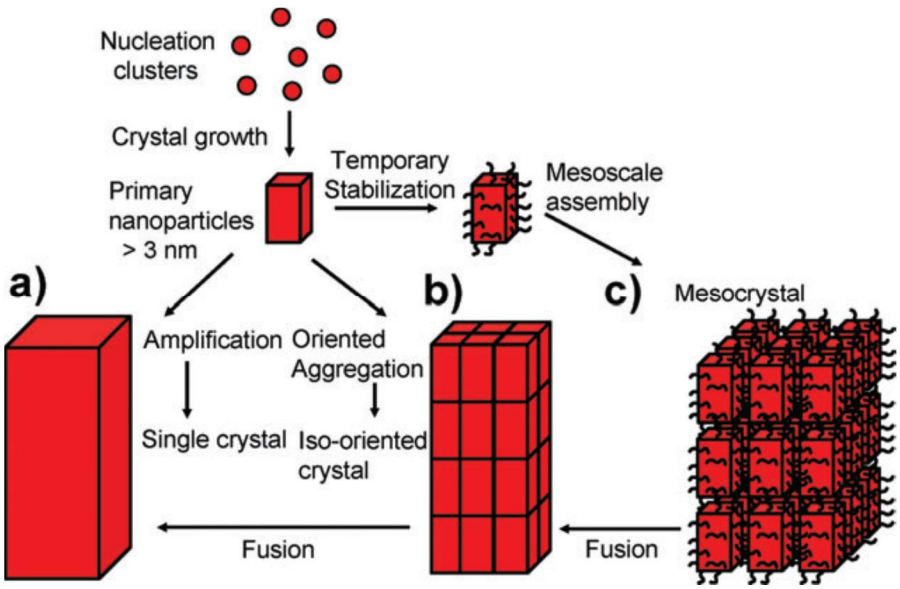

Figure 3 Schematic representation of classical and non-classical crystallization. (a) classical crystallization pathway, (b) oriented attachment of primary nanoparticles forming an iso-oriented crystal upon fusing, (c) mesocrystal formation via self-assembly of primary nanoparticles covered with organic ligands. (*13*)

1.2 In-situ TEM Observation of Non-classical crystallization

Transmission electron microscope (TEM) has enabled the analysis of fine nanometer units by the gain in resolution which is generated by injecting electrons accelerated with high energy. The TEM analysis is very attractive in that direct visual observation can be used as a powerful evidence to reveal the mechanism of a phenomenon. Especially, in-situ TEM is an investigation technique that uses an electron microscope to observe the response of a sample to a stimulus in real time.

Since 1960, the improvement of spatial resolution has been focused on improving the equipment. In addition, the image platform and the specimen stage have also been improved, enabling the observation of atomic resolution in the system. Furthermore, the development of an image system through the charge-coupled device (CCD) and the combination of a special holder capable of external stimulation enable d the observation of the on-system rather than the observation of the simple off-system. Therefore, the in-situ TEM technic is used to conduct experiments involving mechanical, chemical, thermal, and electrical responses.

As mentioned earlier, the non-classical crystallization is reported to occur well in solution system, therefore, liquid cell technic that can create solution environment in TEM is used. Since the analytical method using such a liquid cell must be completely sealed in ultra-high vacuum, much care must be paid to the specimen production. It is common to use silicon nitride and graphene. Using a silicon nitride liquid cell for in situ TEM observation,

Liao et al. carried out detailed real-time imaging to show how Pt_3Fe nanorods grow by nanoparticles in solution. (*14*) (Fig. 4) By in situ TEM observation using graphene liquid cells, Yuk et al. carried out direct atomic-resolution imaging to show how Pt crystals grow in solution. (*15*) (Fig. 5)

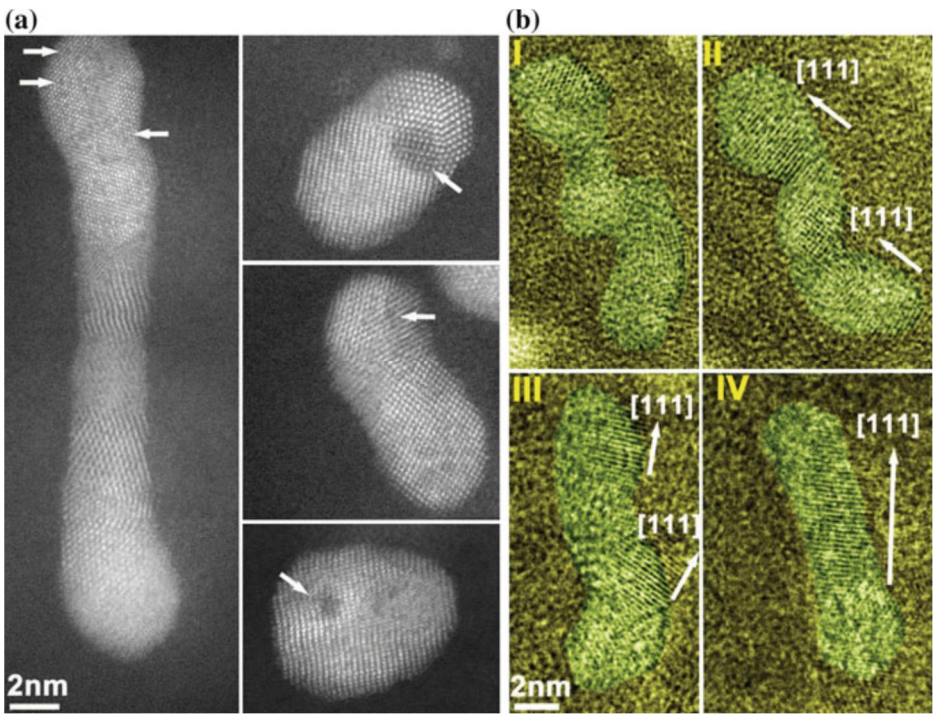

Figure 4 (a) HAADF STEM image of a polycrystalline Pt_3Fe nanorod, dimers, and nanoparticles obtained in a silicon nitride liquid cell. The dark spots (examples highlighted by arrows) indicate the iron-rich regions. (b) Sequential HRTEM images (I–IV) show both crystal orientation and shape changes during the straightening of a twisted nanoparticle chain (*14*)

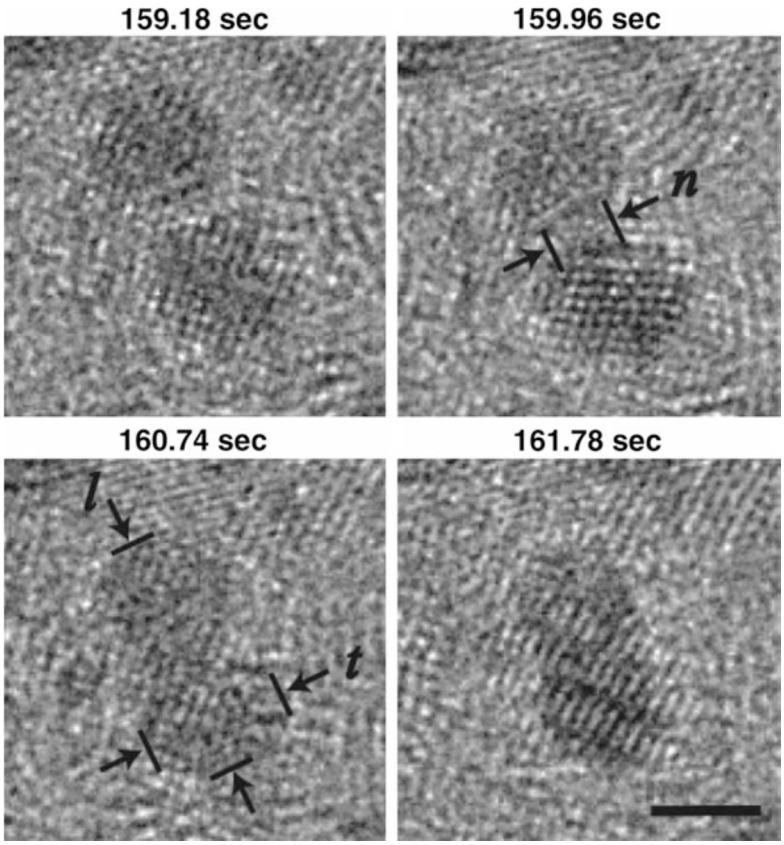

Figure 5 Pt nanocrystal dynamics of coalescence. t and n in the figure represent respectively the length along the center-to-center direction, the thickness in vertical direction to the length and the neck diameter. Scale bar, 2 nm (*15*)

The common finding in these two experiments is that the solution reacts with the electron beam to generate nanoparticles internally, and second, the nanoparticles aggregate together and grow into larger particles or particle chain. In particular, the Pt_3Fe nanorods is formed by nanoparticle

attachment with structural reorientation and rotation, indicating critical mechanisms of the nanostructures growth from nanoparticle building blocks.

These new discoveries are direct evidence of non-classical growth, but all focused on phenomenological observations, and no clear mechanism has been suggested for which factors directly produce nanoparticles and cause coalescence.

1.3 Theory of Charged Nanoparticle

Prof. Hwang studied extensively the non-classical crystallization in the CVD process, publishing about 80 SCI papers during the past decades. (*16-19*) He suggested that the non-classical crystallization can be applied to crystal growth not only in solution but also in the gas phase synthesis of thin films and nanostructures by chemical vapor deposition (CVD) and physical vapor deposition (PVD). In developing this argument, the creative point of extending the non-classical crystallization mechanism from the liquid phase to the gas phase is the existence of charge in the growth system. Briefly, the nanoparticles produced in the gas phase are charged, which acts as a building block in forming the nanostructure. (Fig. 6) This theory as mentioned a 'Theory of charged nanoparticle(TCN)' originated with a puzzling phenomenon where diamond and soot are formed simultaneously under the hot wire chemical vapor deposition (HFCVD) condition in which

diamond is deposited. When silicon (Si), iron (Fe) and palladium (Pd) substrates were placed side by side under the same processing condition of HFCVD, diamonds grew on a Si substrate, highly porous skeletal graphitic soot particles grew on an Fe substrate and carbon nanotubes grew on a Pd substrate as shown in Fig. 7 (a), (b), (c). This result implies that the growth mechanisms of diamond, soot and carbon nanotubes should be closely related to one another. Therefore, if the growth mechanism of soot is understood, such understanding would provide a great insight as to the growth mechanism of diamond and carbon nanotubes. Besides, the microstructure of soot is very peculiar and cannot be explained by any conventional crystal growth theory based on the atomic or molecular unit. Soot is porous and skeletal, being very fragile and weakly connected. The morphology of soot is like the powder compacts formed by landing of particles formed in the gas phase in the conventional CVD process (*20*)

The growth rate of soot on the iron substrate in Fig. 7 (b) is higher than that of diamond on the silicon substrate by more than 10 times. The high growth rate of soot is difficult to interpret by the atomic hydrogen hypothesis because the graphite should be etched by the atomic hydrogen. If the soot is formed by the conversion from diamond by the catalytic effect of the iron substrate, the growth rate of soot should not be higher than that of diamond. The soot formation is not related with the conductivity of the substrate because diamond can be deposited on copper and gold. In the electrochemistry, the hydrogen H+ ions migrate to the cathode, receive their

missing electrons, and bubble up through the solution as hydrogen gas as follows,

$$2H^+ + 2e^- \rightarrow H_2 \qquad \text{(Eq. 5)}$$

This reaction of hydrogen evolution tends to be the slowest and a rate-determining step in overall reactions of electrochemistry. The reason why Pt is used as an electrode is that Pt has a high rate of hydrogen evolution. The rate of hydrogen evolution depends on metals as shown in Table 1. Pd has the highest rate and Pt was next. This means that Pd and Pt have the high rate to give electrons to hydrogen ions. Therefore, the rate of hydrogen evolution is the rate of charge transfer. Pd, Pt, Rh, Ir, Ni and Fe with a high rate of hydrogen evolution are transition metals which have incompletely filled d-orbitals.

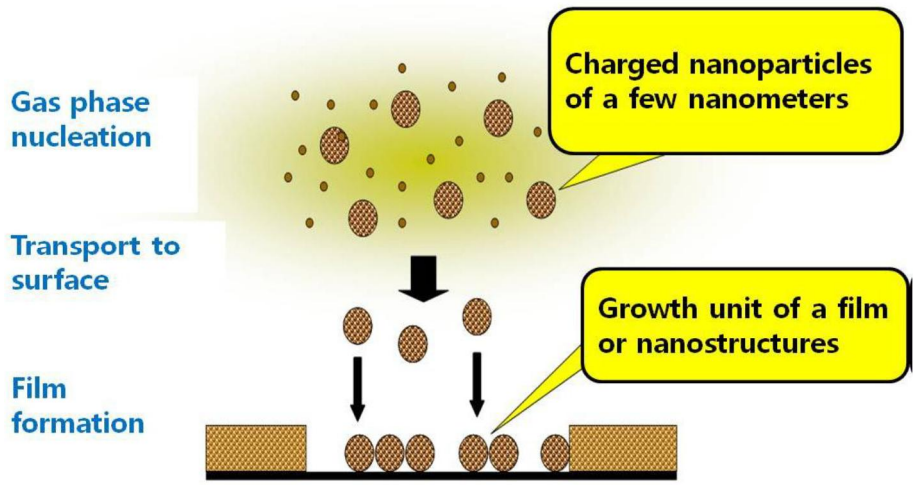

Figure 6 The schematic outline of the ‘Theory of charged nanoparticles’

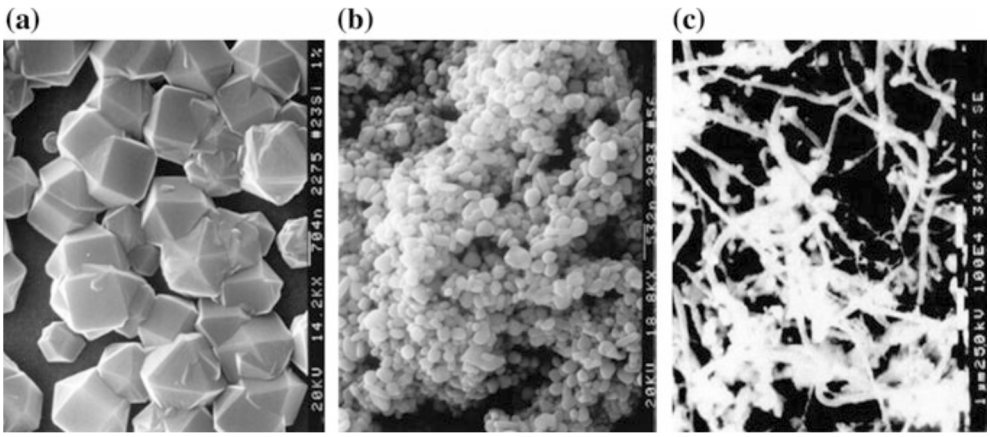

Figure 7 SEM images of (a) diamond deposited on a silicon substrate, (b) soot deposited on an iron substrate and (c) carbon nanotubes (CNTs) on a palladium substrate. The substrates were placed side by side during HWCVD (*16, 21*)

The second proof of charged nanoparticle theory is that soot grows preferentially at the corner of the substrate as shown in Fig. 8. As a result, the soot is developed at the corner. This preferential growth at the corner gives the impression that the soot might be electrically charged because the sharp point like corner provides the high electric field gradient, which would attract the charged species.

Based on these theories, various materials and systems have been set up to demonstrate this phenomenon in many articles. Differential mobility analyzer (DMA) can be used to directly measure these charged nanoparticles. Faraday cups can be used to measure particle size distribution

in the mass. (Fig. 9) A DMA separates charged particles according to their electrical mobility and can be used to produce aerosols of known size and number concentration. Using this system, we confirmed the existence of charged nanoparticles in the growth of nanostructures of Carbon (*22*), Silicon (*23*), Silicon Nitride (*24*), ZnO (*25*), and GaN (*26*), and furthermore, by controlling these particles, the relationship between the electrical sign and the morphology was investigated. (Fig. 10, 11)

Metal	Charge transfer rate (A/cm, log unit)	Metal	Charge transfer rate (A/cm, log unit)
Pd	-3.0	Ag	-5.1
Pt	-3.1	Nb	-5.4
Rh	-3.2	Mo	-5.5
Ir	-3.7	Cu	-6.7
Ni	-5.2	Ta	-7.0
Fe	-5.2	Bi	-8.0
Au	-5.7	Al	-8.1
W	-5.9	Ti	-8.2

Table 1 The rate of the hydrogen evolution reaction on a series of metals at the equilibrium potential (*27*)

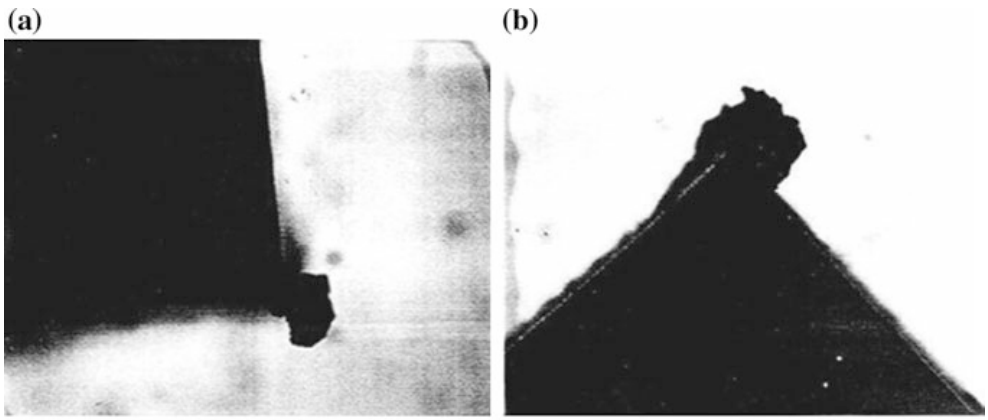

Figure 8 Images of the soot showing the preferential growth at the corner of the Fe substrate

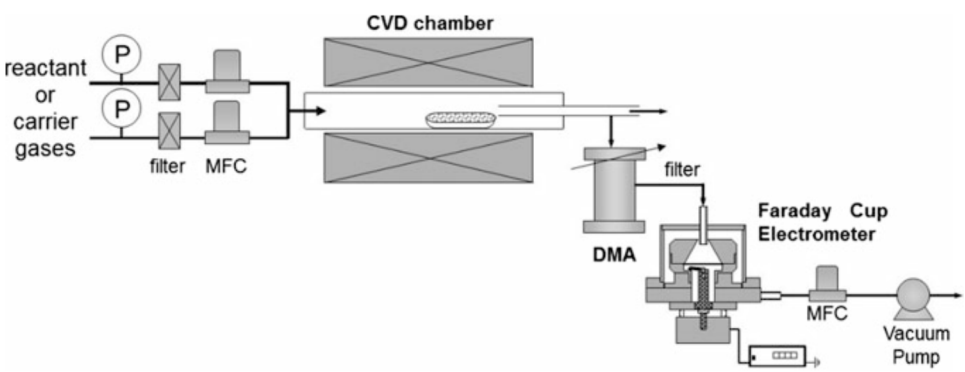

Figure 9 Schematic of experimental set-up for the CVD reactor with the DMA-FCE system for measurements of CNPs generated during atmospheric CVD

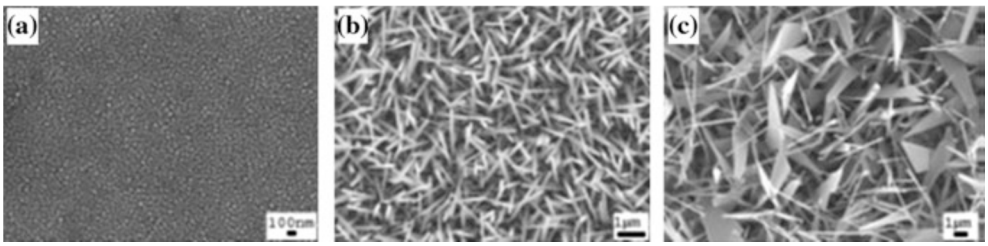

Figure 10 FESEM images of ZnO nanowires at furnace temperatures of a 800 °C, b 900 °C, and c 1000 °C (*25*)

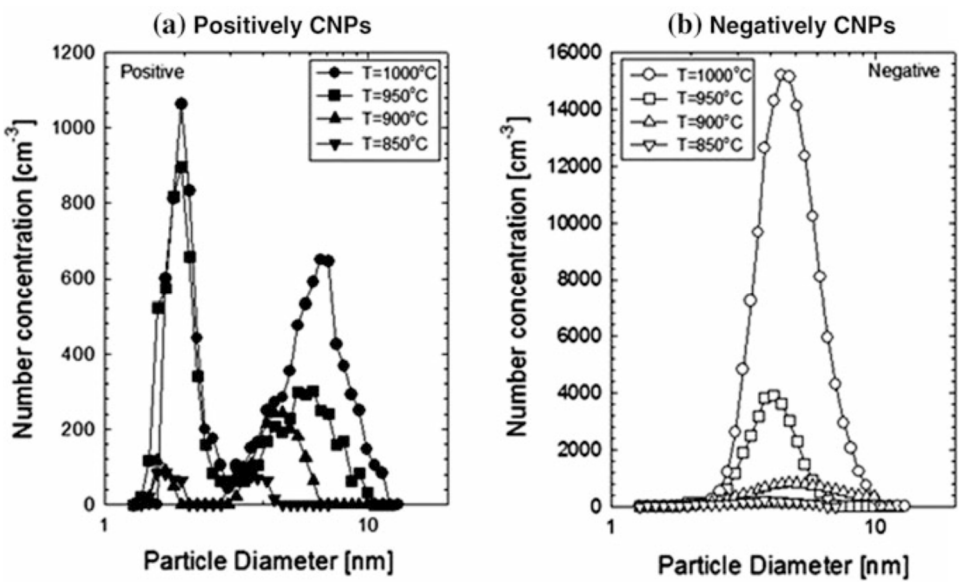

Figure 11 The size distribution of a positively and b negatively charged ZnO nanoparticles at various furnace temperatures (*25*)

1.4 Charged Particle in Transmission Electron Microscope (TEM)

Electrons are smaller than atoms, it should be possible to build a microscope that could see detail well below the atomic level. The image resolution in TEM in terms of the classic Rayleigh criterion, which states that the smallest distance that can be resolved, δ, is given approximately by :

$$\delta = \frac{0.61\lambda}{\mu \sin\beta} \qquad \text{(Eq. 6)}$$

λ : the wavelength of the radiation, μ : the refractive index of the viewing medium, β : the semi-angle of collection of the magnifying lens.

Louis de Broglie's famous equation shows that the wavelength of electrons is related to their energy, E :

$$\lambda = \frac{1.22}{E^{1/2}} \qquad \text{(Eq. 7)}$$

By focusing the accelerated electrons, the TEM allows direct observation of high magnification and high resolution, as well as physical and chemical analysis through various signals generated through reaction with the sample. One of the advantage of accelerated electron radiation is that it produces a wide range of secondary signals from the specimen and some of these are summarized in Fig. 12. Besides providing useful information, the electron beam used in TEM or scanning electron microscope (SEM) can cause

temporary or permanent change in the surface or bulk structure of a specimen. One way of categorizing this damage is in terms of the type of electron scattering that gives rise to it. (Fig. 13)

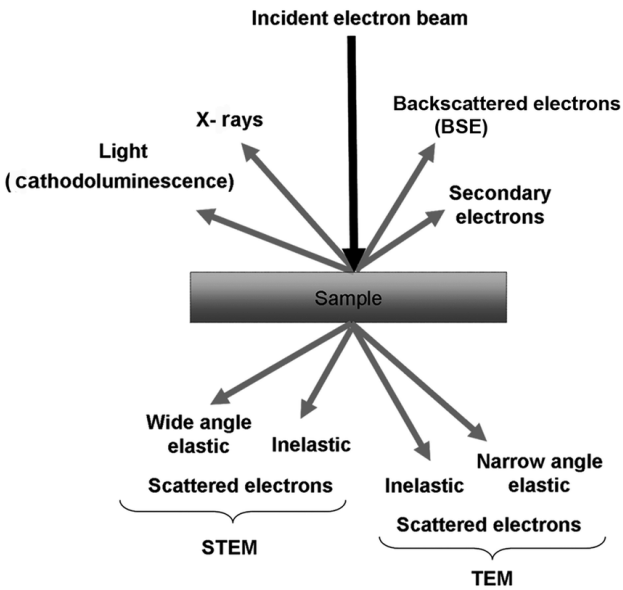

Figure 12 Signals generated when a high-energy beam of electrons interacts with a thin specimen.

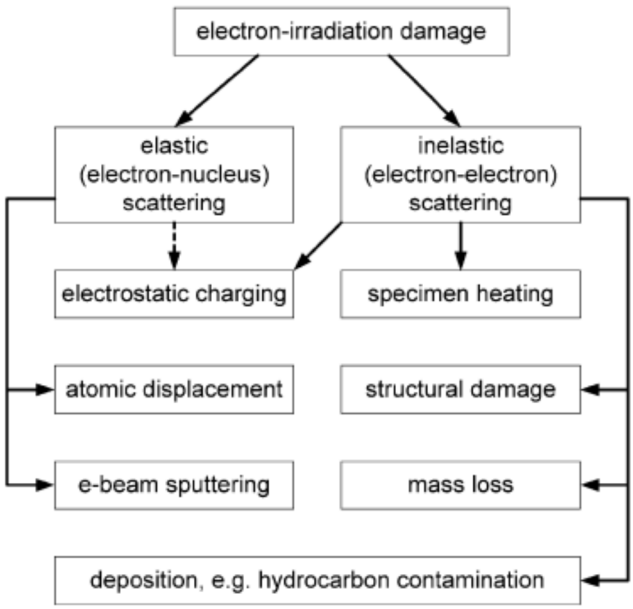

Figure 13 Classification of radiation damage according to the type of electron scattering and according to the effects produced in a specimen. (*28*)

Inelastic scattering represents coulomb interaction of incoming electrons with the atomic electrons that surround each nucleus. It gives rise to the secondary-electron production that provides SEM images, to the emission of X-rays (used for elemental analysis in the SEM and TEM) and to electron energy-loss spectra (EELS) in the TEM. But inelastic scattering can also produce radiolysis effects, which change the structure of a specimen or remove material (mass loss). Under certain conditions (the presence of ambient hydrocarbons), electronic excitation also causes hydrocarbon contamination, which obscures or distorts the TEM or SEM image.

Theses ancillary effects have been suppressed or ignored in the interpretation even if it has occurred during experimental observation. In particular, although the charging can have a significant impact on the system energy for force in the target material, much is not taken into consideration. The same situation holds in TEM where the only macroscopic effect under consideration is often specimen heating. (*29*) The microscopic mechanisms of interest are restricted to those initiated by the ionization of atoms in thin TEM specimens, leading to the emission of secondary and Auger electrons into the vacuum. When non-conductive specimens such as metal oxides are observed using transmission electron microscopy (TEM), secondary electrons are emitted from the specimens, leaving them positively charged. Excess charging can result in morphology changes and specimen drifts, which makes it difficult to conduct accurate TEM observations and analyses. This positive charging is partly compensated by a current of electrons conducted into the irradiated area from the surroundings such as the grid set on the specimen holder. Conversely, if the grid on the specimen holder does not compensate for the electrons, it will be possible to induce an environment in which there is charge inside the TEM.

While standard TEM techniques can reveal sample charging, particularly by defocusing the image, electron holography is capable of directly measuring phase shifts of the incident electron wave caused by uncompensated electrostatic charge in the sample and the associated electric fringing fields. Charging effects in the TEM are of intrinsic interest, but

these effects are detrimental to many types of analysis. (*30*) (*31*)

One interesting experiment was conducted in a recent paper. The degree of charge when electron beam was irradiated on SiO_2 nanoparticles was confirmed by conducting path in TEM. (*32*) The incident electrons illuminated on the particle induce the emission of secondary electrons so that the particle becomes positively charged. Part of these secondary electrons emitted from the illuminated area of the particle and the conducting support film are attracted to the positively charged particle, resulting in discharge from the particle. Secondary electrons emitted from the support film significantly discharge the particle. After the mask shadow completely covered the support film during its forward movement, the amount of charge increased gradually. This means that the discharging by the secondary electrons emitted from the support film still continued, though weak, probably because a part of incident electrons causing Fresnel diffraction hit the support film or secondary electrons emitted from the particle hit the support film causing electron emission. (Fig. 14)

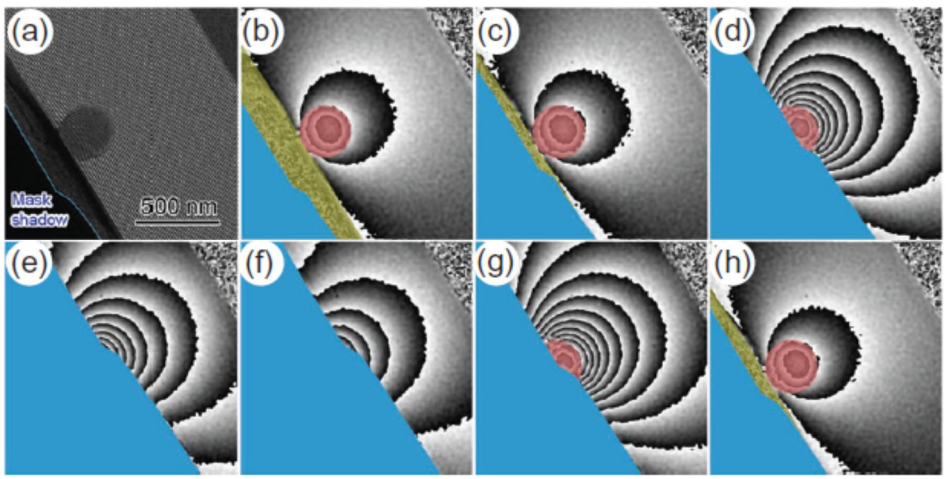

Figure 14 (a) electron hologram and (b) reconstructed phase image of (a). (c-h) Reconstructed phase images as the mask shadow was moved. (Blue : mask shadow) (*32*)

Ch. 2 An isolated Nanoparticle Observation

In classical particle growth, nanoparticles are the smallest growth unit, so understanding this is very important. This is because they have different physical properties depending on the size and shape of the particles. Previously, we have tried to study and apply the equilibrium shape of nanoparticles in order to realize stable functions in various fields. However, nanoparticles are easily altered in shape by less stimulation because of their larger surface area relative to volume. Chapter 2 discusses how charging can also be a factor in nanoparticle instability.

2.1 Structure instability of Nanoparticle

The study of the shape of particles in the nanometer size regime is of great importance for the developments in nanotechnology. Since the 19th century, scientists were able to establish a correlation between the shape and crystal structure. The later discovery of x-ray diffraction allows the establishment of a correlation between atomic ordering and crystalline structure. However, it was clear since the pioneering work of Ino and Owaga (*33, 34*) that nanoparticles assumed shapes and structures different from those of the bulk material. The main reason is the nature of the forces such as surface tension, which act on nanoparticles. Extensive studies

reported in the literature have dealt with the structure and shape of nanoparticles. However, in the nanoworld, the shape is not necessarily constant. (*35-37*)

This is because the energy of a nanoparticle shows many local minima configurations, corresponding to different structures. (*38*) A small excitation (for instance by the beam of an electron microscope) may be sufficient to induce transitions on the particle. (*39*) These phase transitions were first reported by Ijima and Ichihasi (*40, 41*) who found that small gold particles present structural fluctuations. This phenomenon has attracted the attention of several works.(*42*) In order to explain the structural fluctuations two main models have been proposed. The first one involves the complete melting of the particle followed by a recrystallization to a new structure. The energy for the melting is provided by the inelastic scattering of the incoming electrons on the particle. The second model assumes that different particle configurations have similar energies and the low energy barrier between different configurations without melting. This phenomenon has been termed quasimelting by Marks and co-workers and refers to the fluid-like behavior observed in the nanoparticles. (*43*) This liquid-like property is observed by TEM and the effect on charging is referred to as Ijima and Ichihasi (*44*)

Unfortunately, they focused solely on the change of particles on the non-conductive substrate, whereas the opposite conductive particle behaviors were only mentioned and left as objective data. In charged nanoparticle theory, this phenomenon is the most basic data for the behavior of particles

due to charging. Therefore, the goal of this experiment is to reproduce the unstable behavior of particles on a nonconductive substrate, and secondly, We observed the 'sluggish' movement on the conductive substrate in real time and tried to analyze it from the crystallographic point of view.

2.2 Experiment

Au deposition

We have chosen a physical deposition method to avoid controversy of surface conditions due to chemical method such as ligand and surface stabilizer. These additional surfactants can be attached to specific particle surfaces to create unique structure or to prevent aggregation between particles. Therefore, a sputtering method that does not contain any chemical treatment was selected. Au NPs were 2~5nm in size and deposited by metal coater (IB-3 EIKO Co., Ltd, Japan) under conditions of base pressure 0.1 torr, working pressure 0.15 torr, power 500W (2~3 mA) and deposition time 30~45s.

Figure 15 Au metal coater (IB-3)

Substrate selection and preparation

In order to observable the difference in behavior of small particles according to electrical conductivity of substrate, we used amorphous carbon, graphene (few layer graphene) and indium tin oxide(ITO) as conductive substrates and h-boron nitride, silicon monoxide and silicon nitride as insulators. Most of the substrates were prepared from commercially available grids (Ted Pella Co., Ltd., Japan, Prod. #01840 (a-C), 01829 (SiO), 21510-10 (Si_3N_4)), In order to obtain clear information of the particles in the transmission electron microscope, an environment for maximizing the information of the substrate should be created. The best method is to observe the free standing particles, but now we have chosen a way to observe the particles attached to the substrate as a compromise. A commercially sold quantifoil grid is the most suitable grid for this system. The other method was to make the thinner specimens thinner by using an Ion miller and then observed near the thinnest area that was not damaged.

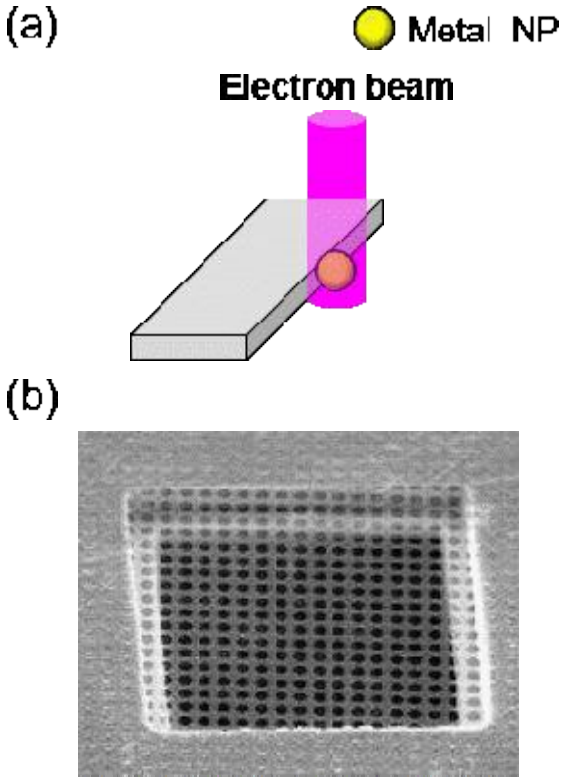

Figure 16 (a) Experiment design (b) Quantifoil TEM grid

TEM observation and video recording

We used a JEOL-2100F TEM at 200kV (JEOL, Col, Ltd., Japan) which is equipped with CCD camera (30 fps). The exposure time was adjusted to 0.1 ~ 0.3s per frame to clearly identify the size and structure of the particles and was recorded using a commercial image capture program. The behavior of the nanoparticles was recorded at low magnification of x150,000 and a high magnification of x1,000,000. The electron dose rate was found to be about 15 ~ 30 pA / cm2, which was detected by the ampere meter connected to the fluorescent plate in TEM. All videos were recording at 908 pixel by 908 pixel resolution.

Image Extraction and Fast Fourier transform(FFT)

To investigate local structural variation from initiation to final of particles, region of interest was selected for Fast Fourier transformation (FFT) patterns as shown in Fig. and Fig. The movies were extracted frame by frame, and then the center of the particle was extracted a square to maximize information about the crystal structure and reducing the undesired background information. The captured image is an RGB (Red-Green-Blue) file consisting of hexadecimal numbers, and the image was converted into binary data for mathematical processing. This frame-by-frame FFT analysis can successfully analyze the instability of the structure taking place in a short time from a crystallographic point of view.

2.3 Result & Discussion

Figure 17 shows the time evolution of an Au NP of ~ 3 nm on an insulating Si_3N_4 substrate. It should be noted that the Au NP is placed not on the top of the substrate but on the edge of the substrate. When Au NPs on the insulating Si_3N_4 substrate are observed, it is difficult to obtain their clear image because of charging and the information overlapping of Au and Si_3N_4 crystal structures. In the initial stage of TEM observations, the image tends to drift due to various reasons and it takes some for the image to stabilize without drift. Only after the image stabilized, the time evolution of Au NPs was analyzed. Figures 17 (a)-(f) show the HRTEM images of an Au NP respectively at the time of 0 s, 0.33 s, 0.66 s, 1 s, 1.33 s, and 1.66 s. Here, 0 s is arbitrary chosen at the time of the analysis. The atomic arrangement changes abruptly after such a short time interval of 0.33 s. In Fig. 17 (a), the atomic arrangement is somewhat disordered. After 0.33 s, however, the atomic arrangement is ordered, indicating a crystalline structure as shown in Fig. 17 (b). In Fig. 17 (c), which is after 0.66 s, the Au NP has the crystalline orientation different from that of Fig. 17 (b). In Fig. 17 (d), which is after 1 s, the Au NP has a stacking fault. Such a dynamic change of atomic arrangements can be also revealed by the FFT image in the inset in the left lower side of each image.

The effect of the electron beam on the dynamic behavior of Au NPs is immediate. In other words, As soon as Au NPs on the Si_3N_4 substrate are exposed to the electron beam during which the image tends to drift, the

atomic arrangement of Au NPs starts to change dynamically. Judging from the fact that the orientation transforms so abruptly, the process appears to be not diffusional but displacive or collective.

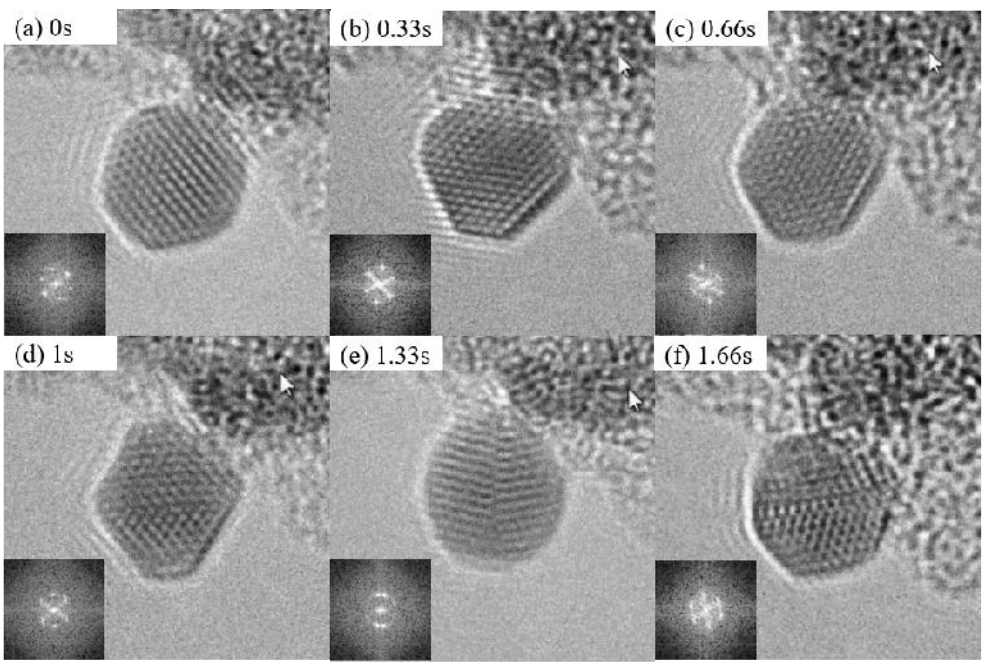

Figure 17 Observation of dynamic behavior of Au nanoparticles on insulating substrate. (a)-(f) has time interval 0.33 s

During TEM observation of Au NPs, occasionally an Au NP falls off from the substrate, which would be attributed to Coulomb repulsion because it occurs only on the insulating substrate. Figure 2 shows such an example. The microstructural change in Fig. 16 indicates that the Au NP is elongated in the [111] direction from the substrate before it finally falls off in Fig. 18

(h). These two phenomena of Figs. 17 and 18 are also observed on other insulating substrates of SiO and h-BN.

Although it is relatively clear that falling off of the Au NP from the substrate shown in Fig. 18 (d) is attributed to Coulomb repulsion, which is again attributed to charging up on the insulating substrate, it is not clear which is responsible for the dynamic behavior of Au NPs in Fig. 17 : electron bombardment or charge. If the dynamic behavior of NPs comes from the electron bombardment, it would also occur on the conducting substrate.

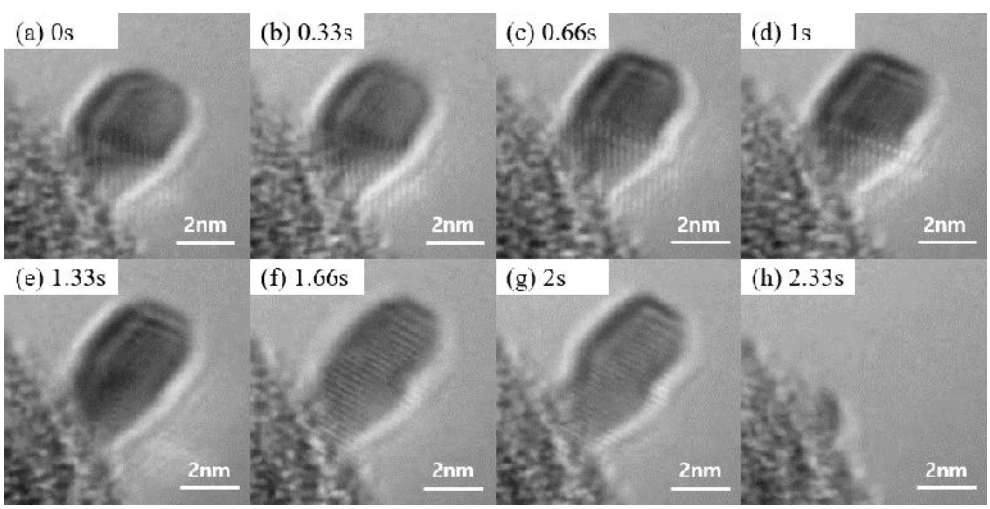

Figure 18 Extraction of nanoparticle due to electrical coulombic force. (Time intervals : 0.33s)

However, an Au NP on the conducting amorphous carbon substrate in Fig. 19 does not show any orientation fluctuation at all, whose behavior is highly in contrast with Fig. 17 and Fig. 19. Figures 19 (a) – (f) show the HRTEM images of an Au NP respectively at the time of 0 s, 2 s, 4 s, 10 s, 30 s and 60 s. The initial orientation in Fig. 19 (a) is maintained throughout the observation. More specifically, when the Au NP was observed on the [1 0 0] zone axis, the edges of the (1 1 1) and (0 0 2) planes were clearly maintained as shown in Fig. 19. The Au NP in Fig. 19 (f) is elongated by 2 atomic layers, indicating that the Au NP should grow by the addition of Au atoms or cluster nearby between 30 s and 60 s of observation. Similar behavior to those of Fig. 19 is also observed on other conducting substrates of graphene and ITO.

Although Au NPs on the conducting amorphous carbon substrate are exposed to the same environment of electron beams as those on the insulating Si_3N_4 substrate, the orientation fluctuation behavior of Au NPs is drastically different between insulating Si_3N_4 and conducting amorphous carbon substrates. Therefore, the orientation fluctuation of the Au NP in Fig. 17 would not be attributed to the electron bombardment. The amount of charge built up in Au NPs on the insulating substrate would be much larger than that on the conducting substrate. It appears that the larger amount of charge built up in Au NPs on the insulating substrate is responsible for the orientation fluctuation.

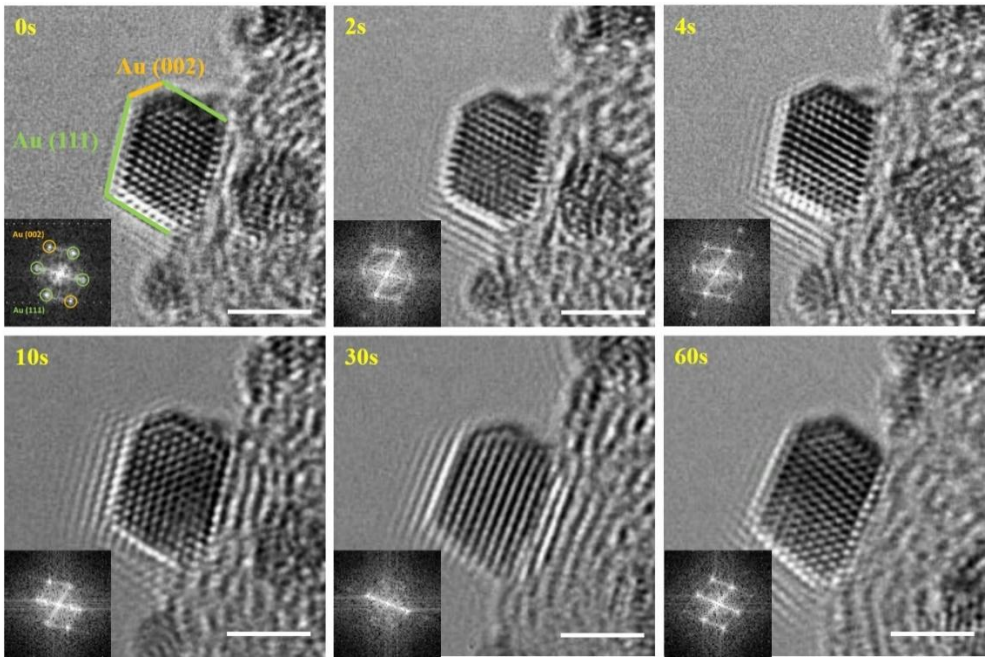

Figure 19 Observation of dynamic behavior of Au nanoparticles on conducting substrate during 1min. (zone axis is [1 0 0], Scale bar : 2nm)

As in Fujita's study on the magic size in the transition from crystalline to amorphous phase induced by electron irradiation of TEM, charging of the sample is inevitable during TEM observation. Therefore, if charge really enhances atomic diffusion of nanoparticles, this aspect will be revealed during in-situ TEM observations. In some literatures surveyed, the role of charge was noticed and mentioned but in other literatures, it was not noticed. In some other cases, the enhanced kinetics was explained by the kinetic energy of electron bombardment. So far, no systematic study has been made

as to the presumption that charge enhances atomic diffusion in nanoparticles. However, there are many experimental results supporting that charge enhances diffusion. One of them was reported by Iijima and his colleagues. More recent results, which are believed to berelated with charge-enhanced diffusion, will be introduced after Iijima et al's works. (*45*)

Ijima and Ichihasi showed a gold particle of ~2 nm size fluctuating between the cubo-octahedral, icosahedral, and single twined structure. In order to induce this effect, particles sitting on an amorphous (usually carbon), or crystalline substrate (usually SiO_2 or Al_2O_3) are exposed to a strong electron beam irradiation with beam intensity between 15 and 80 A/cm^2. The fluctuations of the structure occurs at frequencies of ~10 Hz. A typical series of electron micrographs of the same particle of gold is reproduced in Fig. 18 The change was often accompanied by rotational and translational motion of the particle. They mentioned that the rate of movement was increased by a decrease in the area of the particle in contact with the substrate, which is located at the lower portion of each micrograph. Most importantly, the evolution of the particles, however, became sluggish when an conductors such as α-Fe2O3 was used. Also gold particles supported on a gold film remained inactive without undergoing translational motion or structural fluctuation.

Considering the fact that the evolution rate of particles depends on the conductivity of the substrate, the active movement comes from the amount of charge built up rather than from the electron bombardment. Iijima and

Ichihashi proposed that the state of such a small particle should be called "quasi solid state," which is neither solid nor liquid according to the conventional concepts of matter.

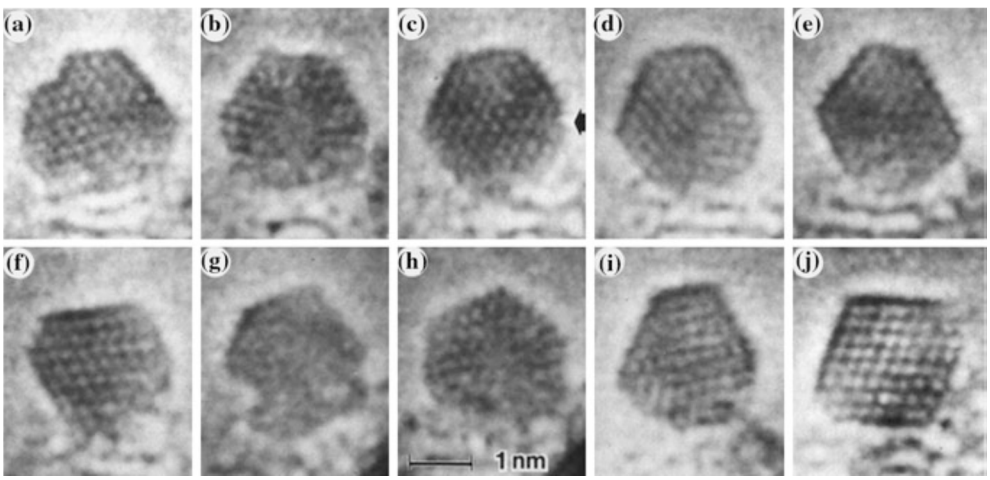

Figure 20 Electron micrographs showing various shapes of an ultrafine particle consisting of about 460 gold atoms reproduced from a video tape recorder. The shape of the particle itself was changing continually under electron-beam irradiation. The lattice fringes appearing in the particles correspond to d_{111} =2.35 Å. The particles in (a), (d), and (i) are single twins. Single crystals with cuboctahedral shape are seen in (e), (f), and (i). From the size of the cuboctahedron (j), the particle theoretically contains 459 gold atoms. The particle also transforms into a multiply twinned icosahedral particle, (b) and (h) (*41*)

Iijima also mentions the change in behavior with nanoparticle size. The reference size is 5 nm, which states that fluctuations of nanoparticles of this size do not occur, and in some articles, particle behavior and coalescence have been confirmed based on this size. However, as shown in Fig. 21, changes in real time crystal structure were confirmed even in a particle of about 7 nm The instability of this large particle is due to the small contact area between the substrate and the particle, so that when the particle migrates to the recessed part of the substrate, the change in crystal structure in the particle is significantly reduced.

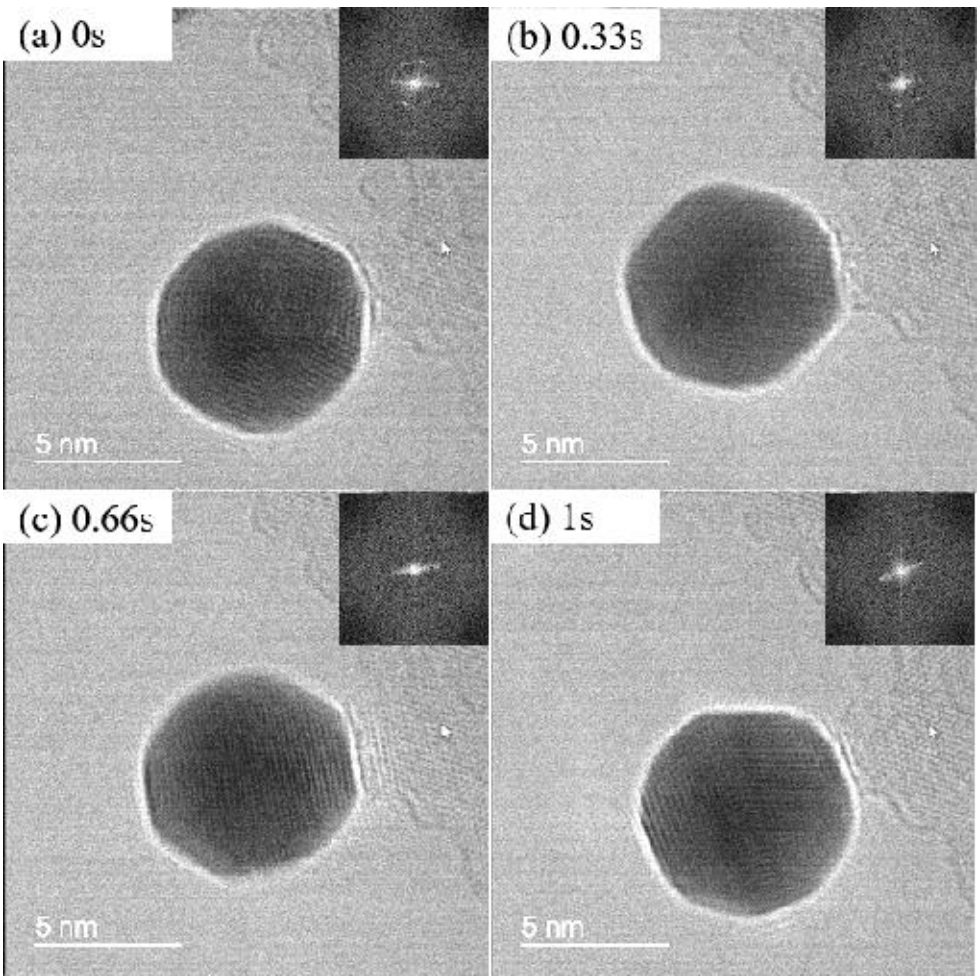

Figure 21 Real-time crystal structure change of 7nm nanoparticles

In the theory of charged nanoparticle, thermodynamically, the Gibbs free energy needs the energy term of electric energy on charged particle case. The Gibbs free energy of formation of a singly charged nanoparticle in gas phase is :

$$\Delta G_{total} = \frac{4\pi r^3}{3}\Delta G_V + 4\pi r^2\gamma + k\frac{e^2}{2r} \qquad \text{(Eq. 8)}$$

K : Coulomb constant, e : electron charge

Figure 22 indicates that the nanoparticles can easily grow up to r' because Gibbs free energy of particle is smaller as particle size is larger in the range of r < r'. And because the particle of radius of r' just need the activation energy of **a** to be the particle of radius of r*, the charged particles can easily grow much larger. These results indicate that charged nanoparticles can be easily generated and grow on hot-wire and plasma CVD processes by ion induced nucleation and the charged nanoparticles are prone to be larger. That is why plasma dust could be easily generated in plasma CVD processes.

These electrostatic energies add additional energy to the system, making the particles unstable and having a liquid-like nature because the charge distribution is constantly changing due to non-equilibrium conditions caused by the irradiated electrons.

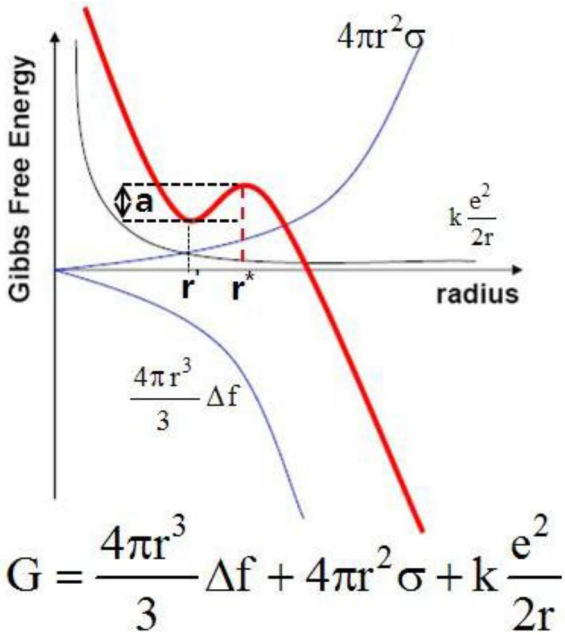

Figure 22 The Gibbs free energy of formation of a singly charged nanoparticle in gas phase (red line).

2.4 Conclusion

The basic element for understanding non-classical particle growth as a theory of charged nanoparticles is to artificially create and observe one charged particle. Inelastic scattering between the electrons and the sample, which have high energies in the TEM, provides an environment in which nanoparticles can become charged. In this experiment, one particle was

observed by controlling the artificial charge environment according to the conductivity of the substrate. The charged particles with charged charges are unstable due to a change in crystal structure or shape in real time, or even separated from the substrate. On the other hand, the uncharged collector shows that the crystal structure does not change despite the long time. This is due to the liquid-like nature of the charged nanoparticles, as the additional electrostatic energy from charge is injected and the energy of the whole system is increased.

Ch. 3 Two or more Nanoparticles Observation

Nanostructures have been studied in a variety of fields because it has extraordinary physical and chemical properties caused by high surface-to-volume ratio as well as it can form complex structures depending on the environment and functionality desired. For this reason, a novel field of material science, chemistry and physics that emphasizes the synthesis and control of nanomaterials has emerged for the past decades. The nature of the nanostructures depends on their size and shape. Thus, how to tailor and control the shape and size of nanostructures and where to apply them is an important issue in nanotechnology. Especially, nanoparticle is a smallest building unit in terms of non-classical crystallization and growth. Therefore, it is necessary to have a clear understanding of how they move and coalesce. Several studies have observed that nanostructures are generated in real-time, and the interpretation of theses phenomena is different. One is interpreted as a permanent dipole (*14*), which is the inherent property of nanoparticles, and the other is interpreted by external factors such as heat (*46, 47*), light (*48, 49*) or surfactants (*50, 51*). In the TEM society, also, the permanent electric dipole moment effect (*14*), the minimization of surface energy (*52*) and the heating effect (*46*) have been proposed. In addition, many mechanisms have been proposed to explain the coalescence phenomenon in the TEM, but it is not clear what is the main factor. As mentioned in the previous chapter, charge causes instability of the particles. This is due to the

increase in the electrostatic energy inside the particle, and it is expected that charge will play a major role in the kinetic of coalescence from a high energy state to a low energy state. Chapter 3 explores and interprets the coalescence phenomena of two or more nanoparticles in terms of charge.

3.1 Aggregation and Coalescence of Nanoparticles

Classically, crystal coarsening has been described in terms of growth of large particles at the expense of smaller particles (Ostwald ripening). The driving force for this process is the surface energy reduction. However, intense research on coarsening behavior and morphology evolution of nanocrystalline structure prepared under growth conditions has led to the formulation of a second mechanism of crystal growth. This so-called attachment mechanism describes the spontaneous self-organization of adjacent particles, so that they share a common crystallographic orientation, followed by the joining of these particles. The process is particularly relevant in the nanocrystalline regime, where bonding between the particles reduces overall energy by removing surface energy associated with unsatisfied bonds. (*5*) (*53*)

Oriented attachment involves spontaneous self-organization of adjacent particles so that they notice and share a common crystallographic orientation each other, followed by contact and joining of these particles. Bonding

between the particles reduces surface energy associated with unsatisfied bonds (through complete elimination of the crystal-air or crystal-fluid interface) This mechanism is relevant in cases where particles are free to move (such as in solution or where particles have abundant surface-bound solution) and probably occurs in nature. It may also apply when particles nucleate side-by-side on a substrate and coalescence during growth. (*11*)

Iijima and Aiayan observed the liquid-like coalescence of small gold particles supported on silica, using HRTEM and real time video recording. (*54*) Particles, which were a few nanometers in size, and decoupled from substrate interactions, coalesced extremely fast, fusing together like viscous droplets in fractions of a second. It is seen from the images that the coalescence of particles of 1–2 nm is completed in a time interval of one frame or 1/60 s, which is the video time resolution available. Direct fusion of still larger particles of 2–3.5 nm occurred in about 1/20 s.

When two particles of 2–3 nm sit firmly on the substrate, the rate of the coalescence is at least two orders of magnitude slower (order of seconds) than that of particles of 1–2 nm not sitting firmly on the substrate. In this case, the lattice fringes of both particles were seen to align even before the particles actually made contact. This alignment means that particles rotate into a lower energy misorientation. The interaction energy between two particles depend on their misorientation when they are close enough. The derivative of the interaction energy with respect to a misorientation angle is a torque, which will rotate the nanoparticles in such a direction as to lower

the interaction energy. Since epitaxial misorientation is expected to have the minimum interaction energy, the rotation would be in a direction to align the lattice fringes of both particles. This rotation would be related with the oriented attachment of particles suggested by Banfield et al. (*3*) As the particle size increases, coalescence occurs during a time interval of minutes and the process occurs in a very similar fashion as in the sintering of micron size particles. A neck is first developed at the plane of contact which is slowly filled by diffusion from the bulk and the surface to the neck region. As the particle sizes get larger, grain boundaries are formed due to the random orientation of the particles before contact. In this case, any fast plastic deformation or structural rearrangements do not occur. Prior to the full-scale experiment, Dr. Kim Hyunmi, who belongs to Professor Kim Ki-bum's laboratory at Seoul National University, initially confirmed the coalescence behavior of charged nanoparticles at low magnification. (Fig. 23) In the 5 hours observation, the feature is that in the amorphous carbon there is no significant change for 30 minutes and then a little coalescence occurs, whereas the gold particles on the SiO are caused to grow through active motion from the beginning. By electrostatic force from the viewpoint of charge, but it is difficult to perform dynamics analysis. Therefore, high-magnification observation is required to confirm the relationship between clear particle instability and coalescence.

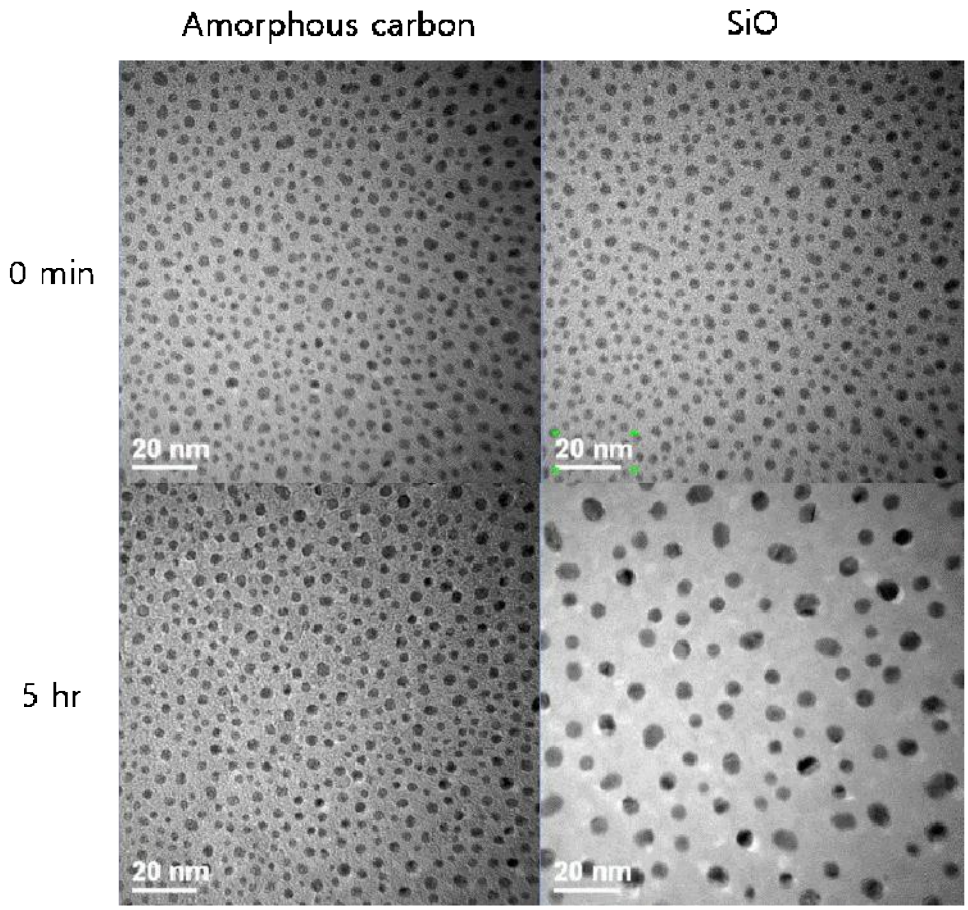

Figure 23 Initial experiments at low magnification of coalescence of Au nanoparticles (unpublished)

3.2 Experiment

Substrate preparation

To observe the coalescence phenomenon, it is necessary to confirm the behavior of a large number of nanoparticles on the substrate because the particles near the edge used for observing the above one nanoparticle can not be used. In the initial experiment, high magnification was observed on the conductive substrate, but the observation was not possible on the non-conductive substrate because the fluctuation of the thin film due to the flux of the electron beam and the continuous interaction between the electron beam and the sample due to charging. This charging phenomenon is commonly observed when observing a non-conductive material using an electron beam. Charges generated in the sample can not escape to the ground, accumulating in the sample, resulting in image distortion and drift due to electromagnetic force between accumulated charge on sample and accelerated electron beam. Therefore, the use of 2-dimension materials has been considered to induce stability of the substrate and local charge only. Graphene and boron nitride have the same hexagonal crystal structure and high thermal chemical stability, and lattice mismatch is very small at 1.7%. It is well suited for this system because it only has different properties for electrical conductivity. (energy band gap : 1.4eV(graphite), 5.97eV(Boron nitride))

The graphene and h-boron nitride were transferred to the lacey grid by mechanical exfoliation method as in a previously published procedure.

(Graphene : SPI Co., Ltd., USA, Grade : SPI-2, h-Boron nitride : Alfa Aesar material Co., Ltd., USA) (*55*) In this transfer process, I tried to eliminate as much as possible the chemical treatment that could affect the experiment. Only acetone and ethanol were used in the silicon wafer cleaning process and transfer, then post-treatment was performed at 200 ℃ to remove residuals. (Fig. 24) In the observation of gold particles on graphene and boron nitride substrate, the zone axis was set to [0 0 2] because the difference in thermal conductivity according to crystal orientation was very large.

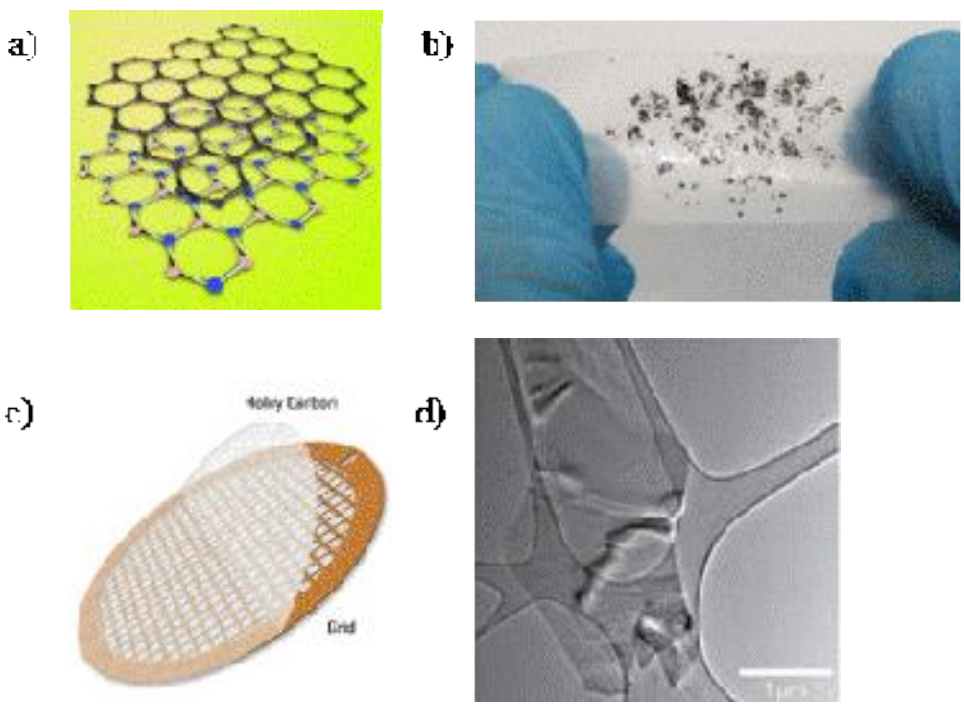

Figure 24 (a) Schematics of graphene and boron nitride sheet (b) mechanical

exfoliation using scotch tape (c) Lacey holey TEM grid (d) Real TEM observation image of graphene on lacey TEM grid

Electron dose calculation

The accelerated electron beam is determined by the amount of charge that the nanoparticles can have, which determines the amount irradiated by the electromagnets within the TEM. Therefore, it is necessary to know the dose accurately in the system so that the correlation of the charged particles with the charged particles can be calculated. The electron is a particle with a negative signal and forms a current according to the flow, and the dose can be confirmed by measuring it. The most common method is to focus the electron beam on a holder with faraday's cup for each TEM and derive the dose by that value, but this can lead to the purchase of additional equipment, although the exact dose can be measured. Recently, TEM has provided a system that indirectly confirm the dose by connecting an amphere meter to a tube plate for observing an image. The JEOL-2010F used in this experiment was also equipped with this system, and electron dose was confirmed based on this system.

The electrons used in the analysis in the TEM are primarily controlled in the condensed lens. Since the range of the appropriate dose to be used for the analysis is generally smaller than the size of the tube plate, the information about the observation area at the beginning of observation in advance. The CCD was used to measure the beam size, and the beam size

was measured step by step, so that a similar dose was applied per measurement.

Coalescence criteria

An essential element in dynamic analysis is time measurement. Since real-time observation is in continuous time, how to interpret the situation is very important. The coalescence phenomenon progresses to initial aggregation, necking, and finally to grain growth. In order to establish a temporal judgment criterion, the time from the initial particle attachment until the final grain growth is selected. (Fig 25) (*56, 57*)

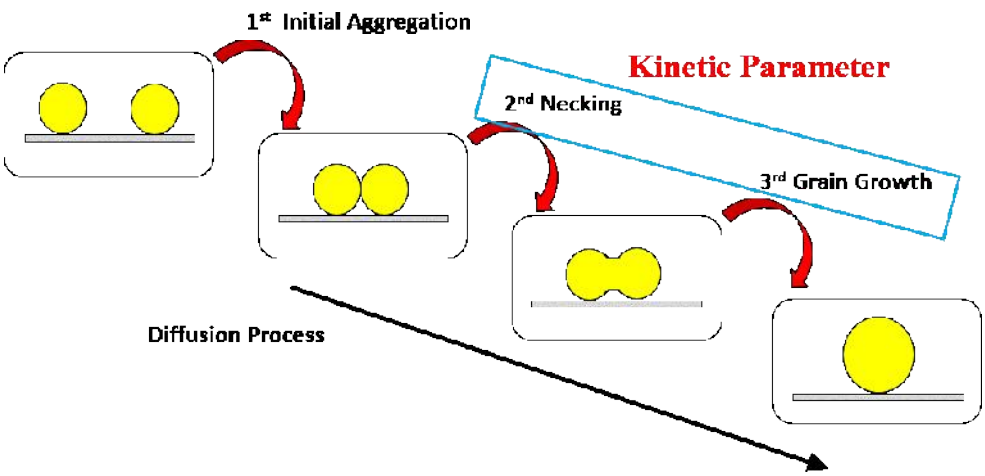

Figure 25 Coalescence time criteria

3.3 Result & Discussion

In order to confirm the consistency of the coalescence phenomenon according to the conductivity of the substrate following the initial experiment, it was confirmed at low magnification on other substrates. As shown in Fig. 26, the same coalescence phenomenon occurs in Si_3N_4 and SiO_2, and it can be confirmed that the saturation is about 30 minutes different from the result of the previous experiment. The difference between these causes;

First, the difference in the measurement conditions due to the use of other TEM. Second, the difference in irradiation dose of electron beam. Third, the difference in the measurement conditions such as the conductivity of the substrate

What is common is that, like the results in chapter 2, the vibrations of nanoparticles are very severe and this movement in unstable energy states creates a coalescence phenomenon.

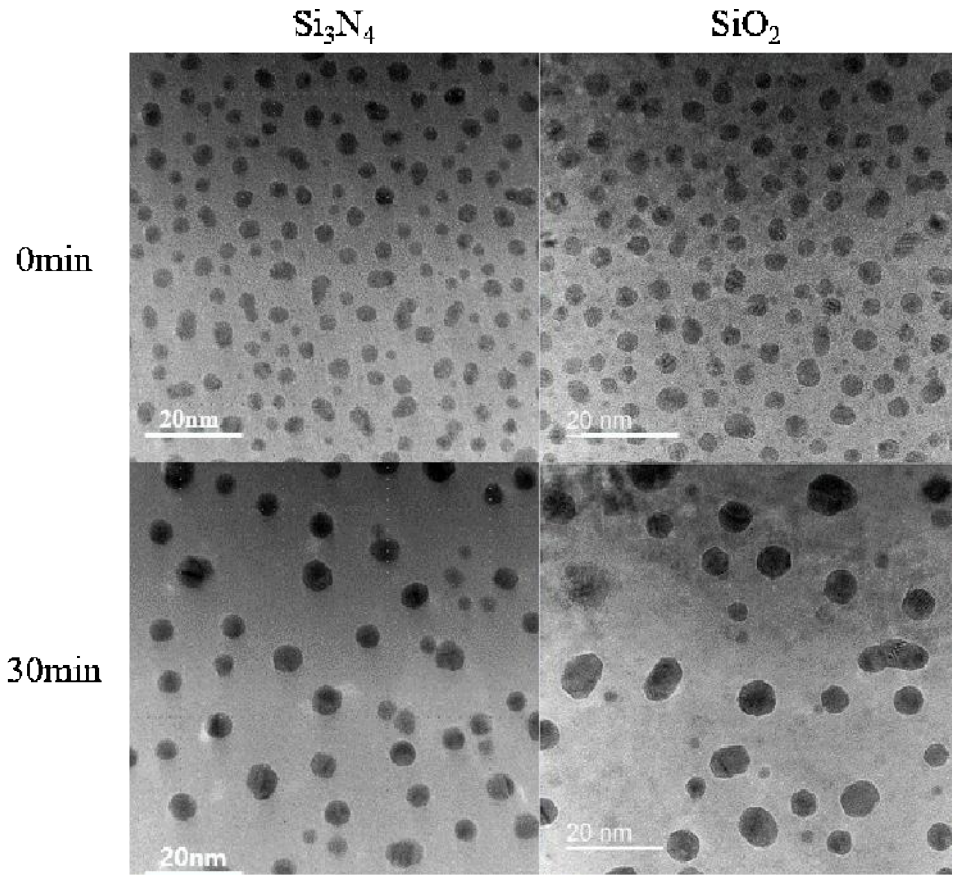

Figure 26 Coalescence of Au nanoparticles in Si_3N_4 and SiO_2

More detail, Coalescence was analyzed dynamically in the TEM and high magnification observations were performed to confirm the mechanism. Fig 27 (a)-(d) shows the time evolution of coalescence of two Au NPs on the insulating h-BN substrate. The coalescence is completed after 0.66 s. In Fig. 27 (a), (b) and (c), the orientation of two Au NPs was different. The particles are initially irradiated with an electron beam, and no coalescence occurs. This is because several factors of the surrounding environment act on the particle, such as when observing one nanoparticle. The coalescence of particles occurs simultaneously after a certain period of time, although each substance is different. Each nanoparticle is randomly fluctuated around its first location and suddenly recognizes and sticks to each other. This takes less than 1 second, and it takes a similar amount of time for SiO_2 and Si_3N_4 injected with the same dose. If there is a correlation between the behavior of nanoparticles and coalescence, and if one nanoparticle is observed, the stable coalescence rate of gold particles is expected to decrease. Figures 28 and 29 show the coalescence time of graphene and ITO substrate, respectively, as in the case of the above nonconductive substrate. Figure 28 (a)-(d) shows the time evolution of coalescence of two Au NPs on the conducting graphene substrate. The coalescence is completed after ~15 s. In Fig. 28 (a), (b) and (c), the orientation of two Au NPs was different.

All coalescence takes place through oriented attachment, a characteristic of conventional non-classical grain growth, regardless of the conductivity of the substrate, which is the bond between the lowest energy faces. It is

important to note that the relationship between the electrical conductivity and coalescence of the substrate is independent of intrinsic properties such as the crystal structure of the substrate. In the non-conductive substrate having an electrical resistance of 10^{13} to 10^{17}, It takes about 15 seconds for a conductive substrate with electrical resistances of 10^{-3} and 10^{-4}. (Table 2)

These temporal differences are maintained in a spherical shape on a geometrically nonconductive substrate, but in a conductive substrate, a worm-like shape is found at an intermediate stage. These temporal differences are maintained in a spherical shape on a geometrically nonconductive substrate, but in a conductive substrate, a worm-like shape is found at an intermediate stage. Considering this physically, it can be interpreted that the diffusion rate and collective motion of the atom are improved. (Fig. 28 (d), Fig. 29(b)-(c))

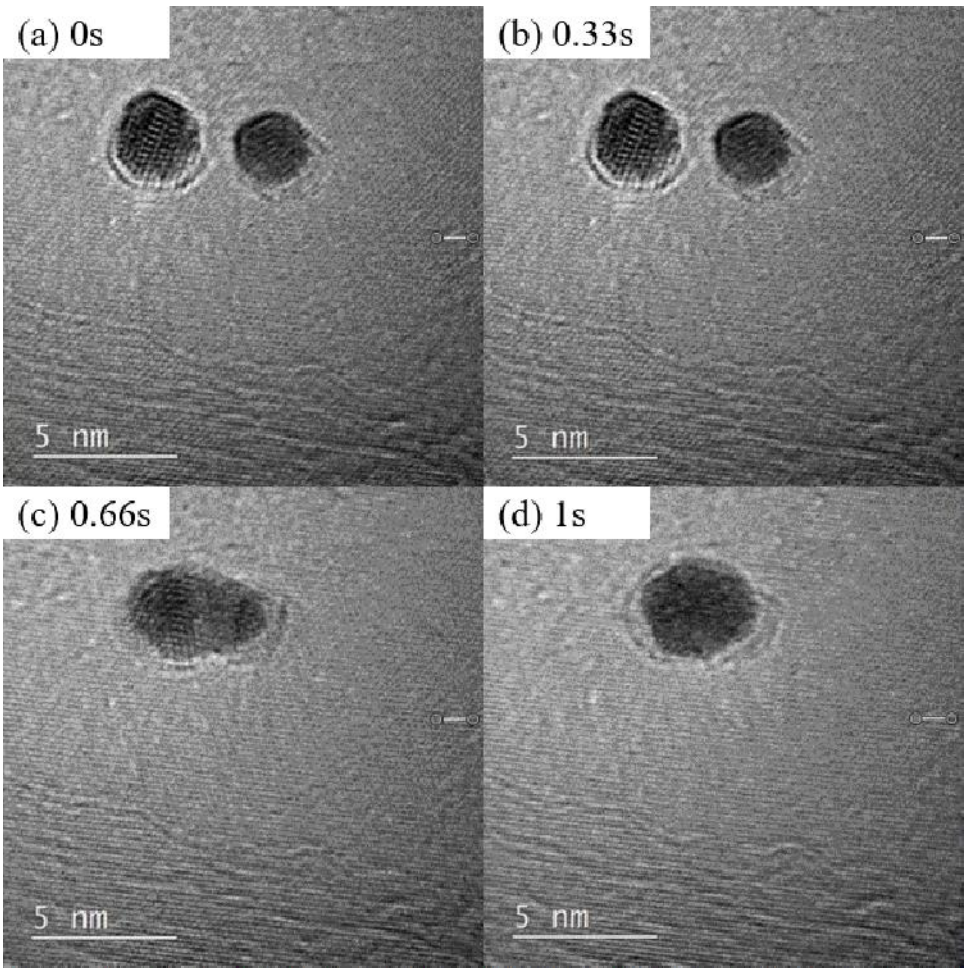

Figure 27 (a)-(d) shows the time evolution of coalescence of two Au NPs on the insulating h-BN substrate. The coalescence is completed after 0.66 s. In Fig. 4(a), (b) and (c), the orientation of two Au NPs was different.

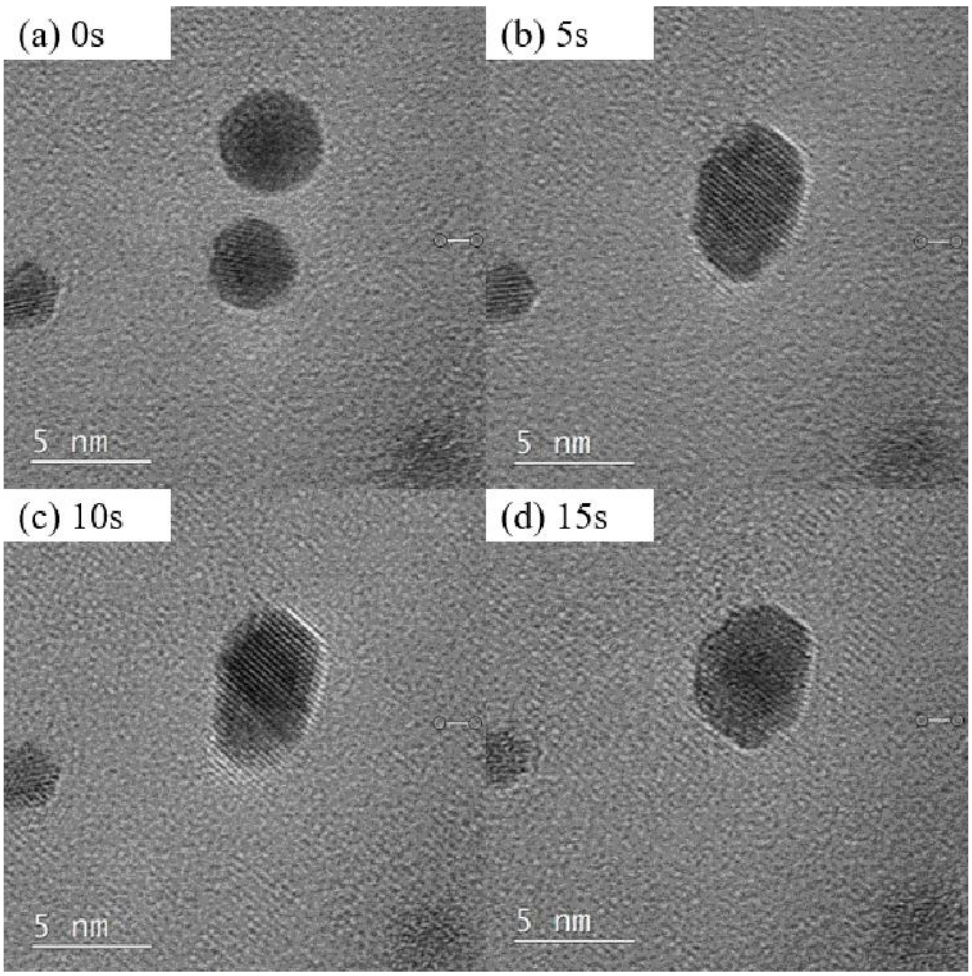

Figure 28 (a)-(d) shows the time evolution of coalescence of two Au NPs on the conducting graphene substrate

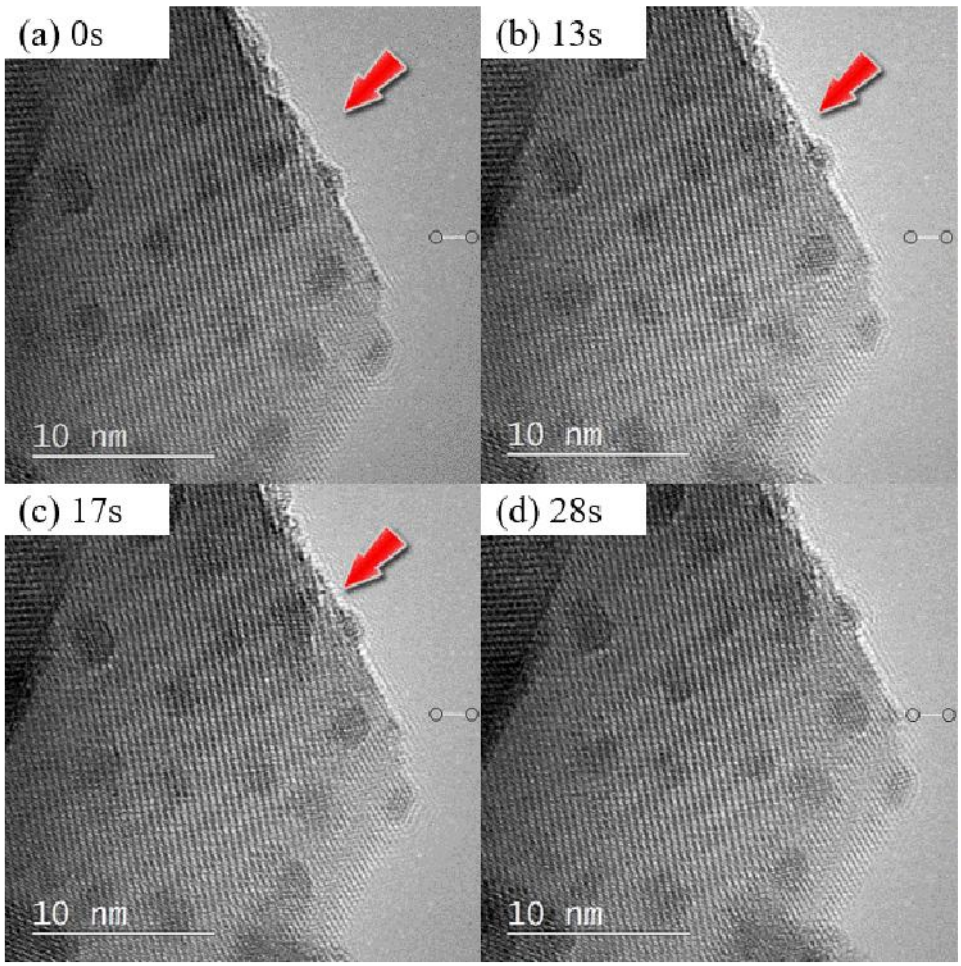

Figure 29 (a)-(d) shows the time evolution of coalescence of two Au NPs on the conducting indium-tin-oxide (ITO) substrate

Substance	Electrical Resistivity (Ω cm)	Average Coalescence time (s)
SiO_2(Film)	$\sim 10^{17}$	< 1
Si_3N_4	10^{13}	< 1
Boron nitride	10^{13}	< 1
ITO (150nm)	4×10^{-4}	~ 15
a-Carbon	3.5×10^{-3}	~ 14
Graphite	3.5×10^{-4}	~ 15

Table 2 Relationship between coalescence time and electrical resistivity.

3.4 Conclusion

The energy of nanoparticles is very unstable due to the external factors that stimulate it because the ratio of surface energy is very high. This increase in energy due to external stimuli causes coalescence phenomenon when multiple particles are present. In this experiment, coalescence of two or more nanoparticles was analyzed dynamically according to the conductivity of the substrate. The time difference of about 15 times according to the change of the substrate depending on the charged state indicates that the electrostatic energy presented when observing the above one nanoparticle was involved in the total energy. In the coalescence of all grains, it was confirmed that oriented attachment, which is a characteristic of non-classical grain growth method, is common. The correlation of similar coalescence time on several substrates is related to the electrical resistance rather than the environment of the substrate, suggesting that charge can have a significant effect on coalescence kinetic.

Ch. 4 Artificial current path systems : Floating & Ground environment formed simultaneously in a TEM grid

As mentioned in previous chapter 1.4, the irradiation of accelerated electron beams with high energy causes deformation of the sample. The main reason for this strain is the temperature rise. Many papers have studied the effect on temperature, but it is not easy to identify it because it only observes the local area. In this study, too, we can not exclude the effect of temperature, so we tried to check the effect of temperature on cryo-TEM.

The following problems can be raised because various types of substrates have been used to verify the effect of charging in previous experiments. This diversity has been chosen to focus on the conductivity of the substrate, but it is difficult to make the environment where the targeted gold particles are placed fair. The most disturbing factors in the movement of particles are the contact angle problem due to the degree of bonding with the substrate, and the hydrocarbon contamination due to the time difference of observation. (*58*)

Finally, for generalization, the diversity of materials must also be pursued. Silver is a transition metal having similar properties to gold, and this was selected to extend the range of previous experiments limited to gold to demonstrate the charging effect.

4.1 Controversy over the observation of charged nanoparticles using in-situ TEM

Heating

Deformation of the sample in TEM observation can not be correlated with temperature. This is because the phonon occurs in the reaction between the electron beam and the sample. There are many papers that describe the reaction and deformation of a sample in relation to temperature, while someone insisted that the physical calculations and observations by indirectly melting a substance with a low melting point and observing that the temperature does not have a significant effect during sample observation.

The temperature rise of amorphous carbon film resulting from electron beam heating has been estimated according to the Eq. (eq. 9) ΔT is the value of temperature rise, I is the beam current, κ is the thermal conductivity, e is the electron charge, b is the radius of the heat sink, r_0 is the beam radius and ΔE/d approximately equals to dE/dx acquired from Bethe formula (eq. 10, 11)

$$\Delta \mathrm{T} = \frac{I}{\pi \kappa e}\left(\frac{\Delta E}{d}\right) \ln \frac{b}{r_0} \qquad \text{(eq. 9)}$$

$$\frac{dE}{dx} = \frac{4\pi}{m_e c^2} \cdot \frac{n}{\beta^2} \cdot \left(\frac{e^2}{4\pi\varepsilon_0}\right)^2 \cdot \left[\ln\left(\frac{2m_e c^2 \beta^2}{I_e \cdot (1-\beta^2)}\right) - \beta^2\right] \qquad \text{(eq. 10)}$$

$$n = \frac{N_A \cdot Z \cdot \rho}{M_\mu} \quad \text{(eq. 11)}$$

The rate of energy loss dE/dx depends on the atomic number (Z), density (ρ) and the approximate mean excitation energy (I_e) of the sample, and the velocity of electrons (v). N_A is the Avogadro number, M_μ the Molar mass, c is the speed of light and ε_0 the vacuum permittivity, $\beta = v/c$, and m_e the rest mass. The maximum temperature rise of amorphous carbon film calculated by the Eqs. (9–11) is 80 K. This value is very similar to the value IiJima indirectly observed by observing Bi. They tried to estimate the cluster temperature by other methods. Firstly, Bi clusters were prepared and observed in exactly the same procedure as the Au clusters. The results confirmed a solid state of the Bi clusters, since they exhibited lattice fringe images. This means that the substrate temperature during the observation in the microscope would not exceed the melting temperature of Bi which is 271 °C. Secondly, to examine an effect of the electron beam heating, conventional and micro-beam modes in electron microscopic observations were compared in terms of the probe size. There was no major change in cluster activities. A cluster temperature was determined by a balance of heat dissipation through conduction and heat gain through inelastic scattering events of the incident electron beam in the cluster. The cluster temperature was estimated to be almost the same as that of the substrate, which is room temperature.

Sample condition, Hydrocarbon and TEM observation condition

Electron beam-induced specimen contamination in the transmission (TEM) has remained a problem since the beginning of these forms of microscopy. Sources of contamination can be attributed to one or a combination of three major contributors: 1) the pumping system, 2) other internal SEM component parts (i.e., specimen stage, stage lubricants, O-rings, etc.), or 3) the sample (including its preparation and handling). There are many efforts to suppress this, but it is not easy to control because of the complexity of the elements.

In addition, the TEM observation depending on the presence or absence of charge may change the condition of the electron beam due to the time interval of measurement. In particular, when charged, the beam must be continuously controlled to compensate for drift and drift caused by interaction between the electron beam and the sample. Therefore, there is a difference from the stable observation condition when observing the conductive material.

Contact area

The use of various substrates places a great deal of controversy on the difference in conductivity in their choice. Among them, the most important concern is the contact area, which is a large part of the nanoparticles, which is attached to the substrate. The use of various substrates places a great deal of controversy on the difference in conductivity in their choice. Among them, the most important concern is the contact area, which is a large part of

the nanoparticles, which is attached to the substrate. The higher the ratio of the contact area to the total particle size, the more the particles resist movement.

Target material

The previous results are all designed and observed for gold particles. In order to generalize the theory of charged nanoparticles and to clearly indicate that charge is an important factor in the formation of nanostructures, it should be confirmed in various systems. The silver, like gold, can be deposited in the same sputter method as a transition metal and can have high purity, so it can be extended to metal particle categories in the application of charged nanoparticles theory.

4.2 Experiment

Cryo-TEM Observation

To confirm that the collective motion is improved by the charge excluding the temperature, the behavior of the nanoparticles should be confirmed at extremely low temperatures. Cryo-TEM is an analytical technique that can be observed at liquid nitrogen temperatures, allowing observation at extreme low temperatures. (-178℃) At this temperature, the behavior of gold particles on the SiO substrate was confirmed in real time. This measurement

was done using a cryo-TEM holder on a Technai F20 at KIST (Korea Institute of Science and Technology) and the temperature was read by direcly connecting the thermos-couple in the holder to the temperature measuring instrument. Unfortunately, there was no video recording program at that time of measurement, so we used an artificial measurement device to capture the exposed monitor.

Floating and Ground

What distinguishes floating and ground is whether an artificially generated current can flow toward the ground. The motif of this experiment comes from Dr. Youn's experiment, which he demonstrated in indirectly charged nanoparticle theory in the carbon system. he also compared the deposition behavior between electrically floating and grounded silicon substrates, which showed that silicon nanowires grew on the floating substrate whereas nanoparticles grew on the grounded substrate. (Fig. 30) (*59*) These results indicated that the charged nanoparticles that were generated in the gas phase played important role on formation films and nanostructures. The charging of nanoparticles could also make the carbon cluster easily be diamond because the surface energy of diamond can be less than that of graphite on charging situation. The electrical double layer can decrease the surface energy of diamond more than graphite because the former is dielectric and the latter is conducting. This reduction surface energy of diamond causes that diamond particles are more thermodynamically stable than graphite. (*60*)

The main point of this experiment is whether we can artificially adjust the current path and implement it on a single grid. Figure 6 shows the schematics and low magnification TEM images of the experimental design for floating and grounded graphene flakes. Figure 30 shows the schematic of the whole

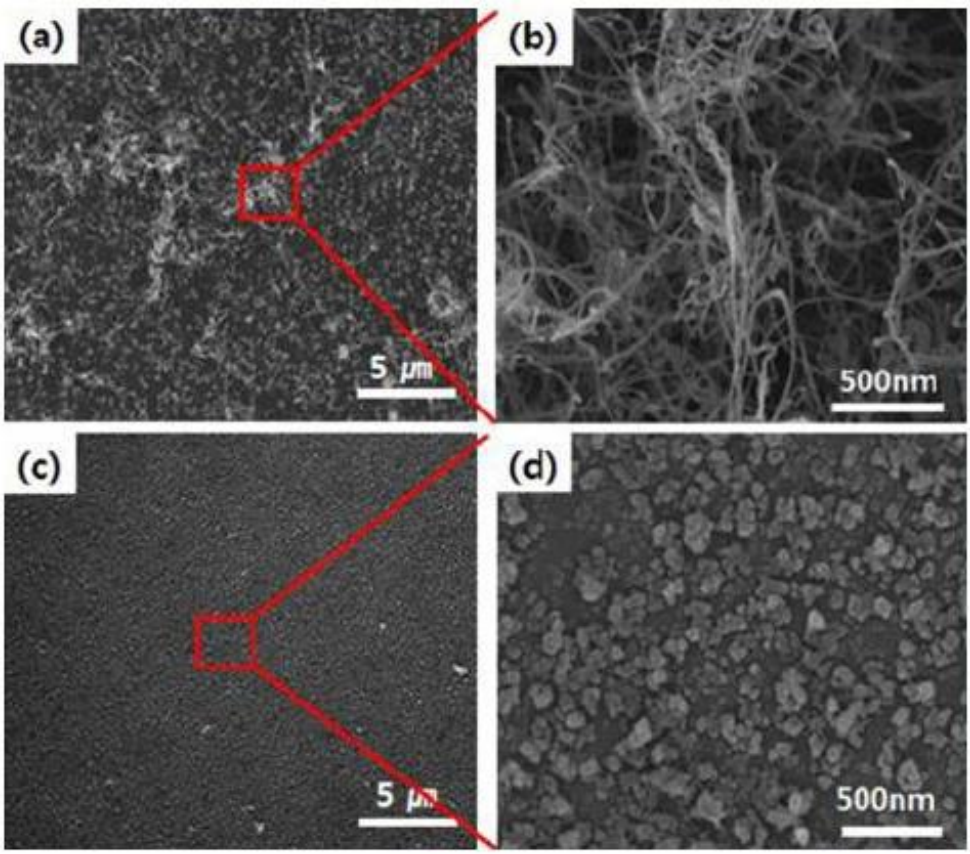

Figure 30 FESEM images: (a) low-magnification and (b) high-magnification images of a floating silicon substrate and (c) low-magnification and (d) high magnification images of a grounded silicon

substrate. (*59*)

copper grid, indicating that both floating and grounded graphene flakes were prepared on the same copper grid and observed under the same TEM environment. Figure 30 (a) shows the schematic, in which the graphene flake is placed on the SiO membrane supported by the copper mesh. It should be noted that the flake is not in contact with the copper mesh. The electron beam is focused on the small area in the boundary between graphene and SiO. Figure 31 (c) shows the TEM image of the graphene (grey) on the SiO membrane (white) and the copper mesh at the upper edge (black). Figure 31 (b) shows the schematic, in which the graphene flake is placed on the SiO membrane but in contact with the copper mesh. Since the copper mesh is electrically grounded, the graphene flake is grounded. Figure 31 (d) shows the TEM image of the graphene (grey) on the SiO membrane (white) and the copper mesh at the lower right (black). Between graphene and SiO was marked by the dashed line.

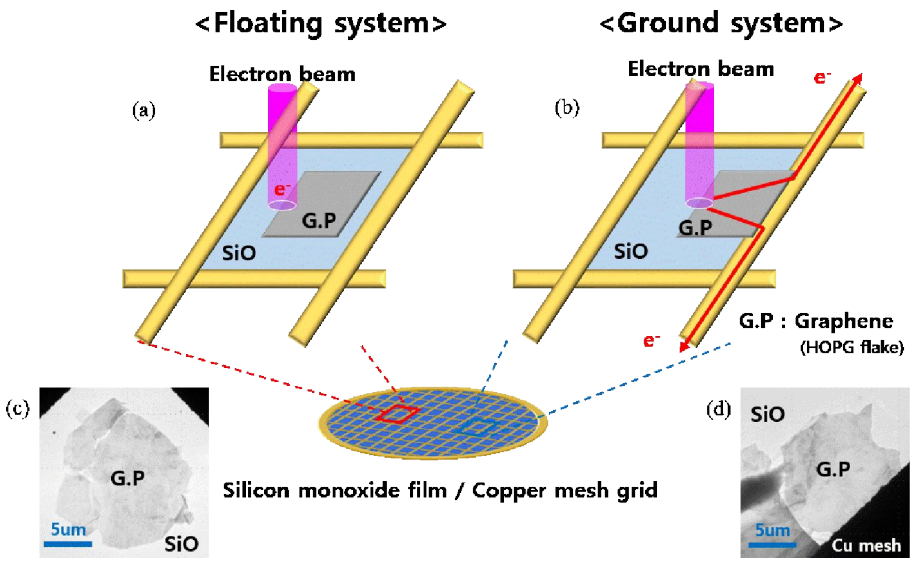

Figure 31 A schematic of artificial charging systems construction (Left) Floating system (Right) Ground system.

Ag deposition

Ag nanoparticles were deposited using sputter method to avoid the possibility about deposition method like synthesis which use the organic ingredient. The direct current (DC) sputter set in the laboratory was used for the deposition of Ag, and the process condition used were as follows; target size : 3 inch (thickness : 1.4 inch), gas source : Ar (30 sccm), base pressure : 8.0×10^{-7} torr, working pressure : 10 mtorr, d.c. power : 20 W, deposition time : ~ 5 s. The size of the Ag nanoparticles deposited under these conditions is approximately 5nm.

4.3 Result & discussion

The expectation of the cryo-TEM experiment is that when the behavior of the particles in the diffusion aspect follows the arrhenius distribution, lowering the temperature will result in a comprehensive increase in the activation barrier, so that coalescence will not occur if this phenomenon is dominated by temperature. As a result of figure 28 shows the images per second by observing the behavior of gold particles measured at liquid nitrogen temperature in real time. Even though it is extremely low temperature, it takes about 6 seconds to coalescence when applying the criteria set out in chapter 3. The transfer of matter is governed by the temperature gradient in the Boltzman distribution, which can be explained by the Arrhenius equation.

$$\mathrm{k} = \mathrm{A} \cdot \exp\left(-\frac{E_a}{kT}\right) \qquad \text{(eq. 12)}$$

Applying this to the movement of the atom should not cause a change in the movement of the gold particles at low temperatures. Although coalescence is slower than the time measured at room temperature, the phenomenon of coalescence can be thought of as external factors other than temperature, and it is a result of proving that charge is applied in the system based on previous results.

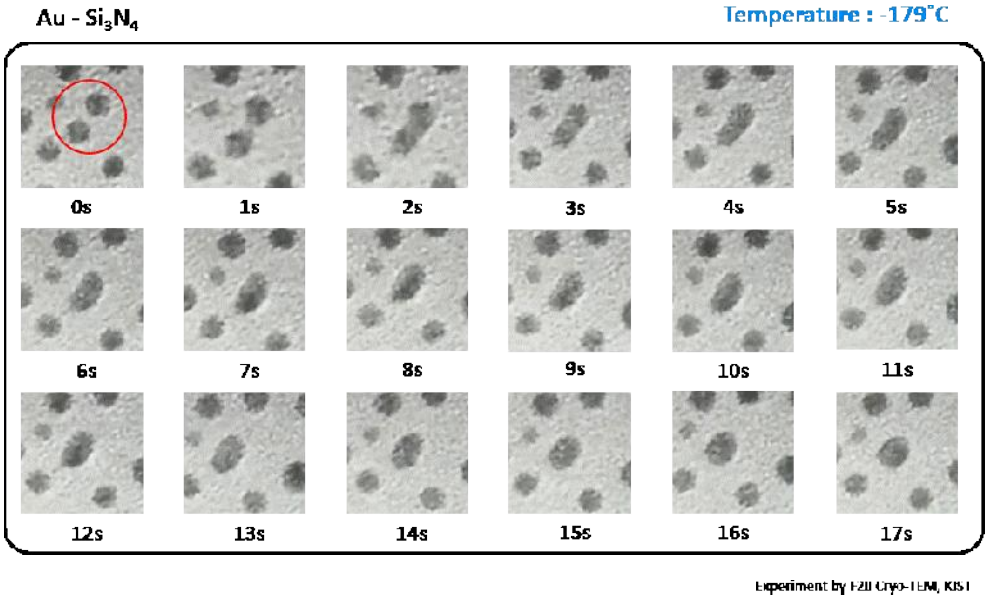

Figure 32 Coalescence of gold particles at liquid nitrogen temperature (-179℃)

Next, we observed changes in the floating and ground system, which eliminated many of the controversies that might have been raised during TEM observations. Figure 33 show the ground system with SiO and Graphene regions separated by a red dashed line. Although the size difference of the deposited particles is subtly existent, the coalescence in terms of energy is advantageous as the radius is small, so if the difference according to the charge is clear, this part will not have a great influence. Figures 33 (a)-(d) show the time evolution TEM images of Au NPs on the grounded graphene and the SiO membrane respectively at 0 min, 5 min, 10 min and 15 min. The boundary between graphene and SiO was marked by the dashed line. Although coarsening by coalescence between NPs was noticeable on SiO but negligible on the grounded graphene up to 15 min. After 15 min (Figure 33(d)), there was a big difference in the size of Au NPs between SiO and graphene.

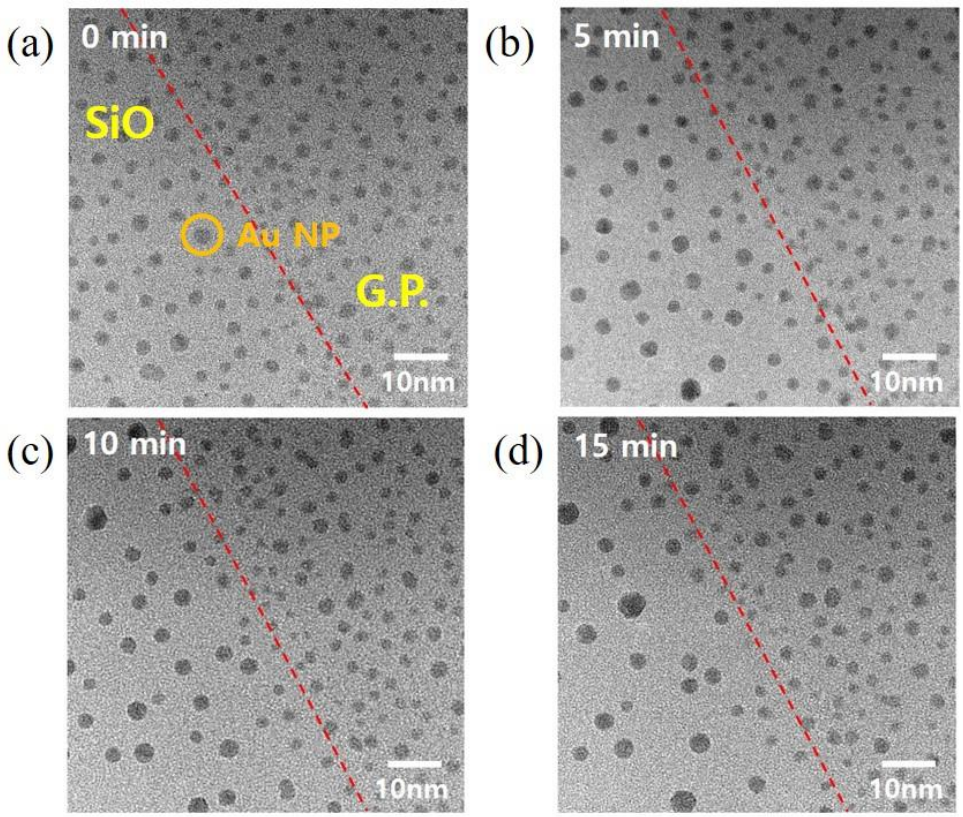

Figure 33 (a)-(d) show the time evolution TEM images of Au NPs on the grounded graphene and the SiO membrane respectively at 0 min, 5 min, 10 min and 15 min.

Figure 37 (b) shows the low magnification TEM image on the grounded graphene and the SiO membrane, showing the spherical area exposed to the electron beam and the adjacent area not exposed to the electron beam. Figure 35 (b) shows how the number density of Au NPs varies with time on the grounded graphene and the SiO membrane. The number density on

graphene decreases only slightly with time but the number density on SiO decreases much more significantly with time.

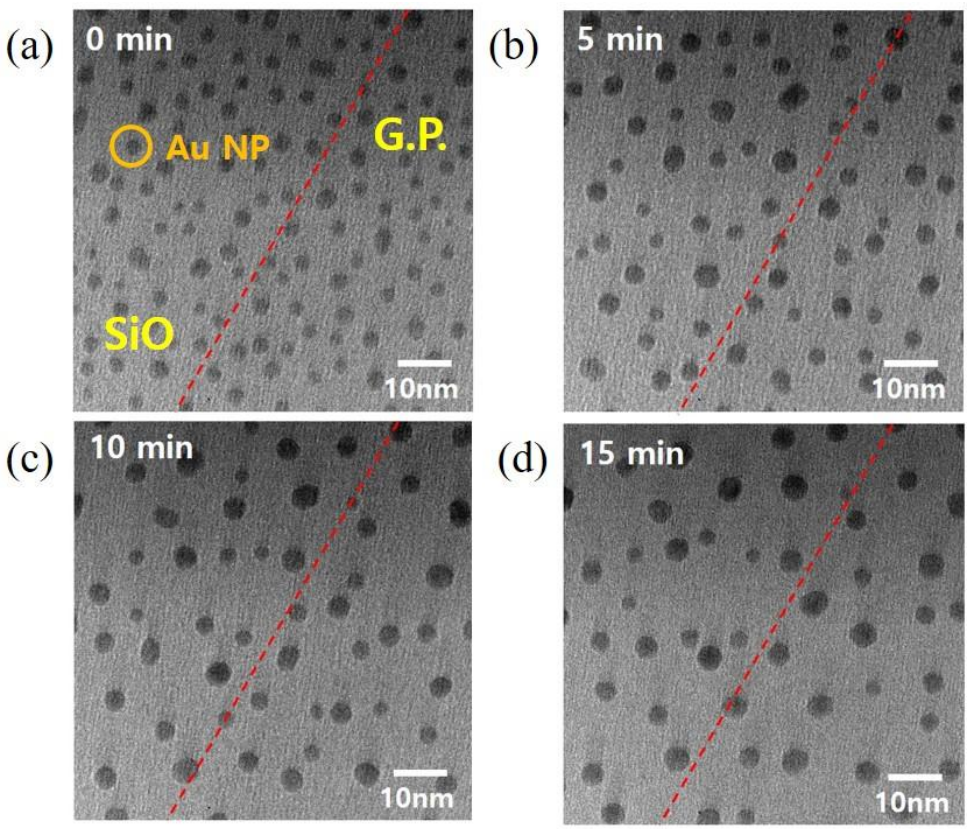

Figure 34 (a)-(d) show the time evolution TEM images of Au NPs on the floating graphene and the SiO membrane respectively at 0 min, 5 min, 10 min and 15 min.

In the floating system, as shown in Fig. 34, the size difference of the particles is not large compared to Fig. 33. Coarsening by coalescence between NPs was noticeable during TEM observation up to 15 min on both graphene and SiO. As a result, the size difference of Au NPs was not distinguished between graphene and SiO. Also the dynamic fluctuation behavior of Au NPs was not distinguished between graphene and SiO, which can be confirmed by the movie.

Such coarsening behavior occurs only in the area exposed to the electron beam as shown in Figure 34. Figure 37 (a) shows the low magnification TEM image on the floating graphene and the SiO membrane, showing the spherical area exposed to the electron beam and the adjacent area not exposed to the electron beam. Figure 35 (b) shows how the number density of Au NPs varies with time on the floating graphene and the SiO membrane. The number density on graphene and SiO decreases with time in a similar way.

These experimental results show that the dynamic fluctuation and coarsening kinetics of Au NPs on the floating graphene are as significant as those on SiO whereas the dynamic fluctuation and coarsening kinetics of Au NPs on the grounded graphene is much more slight. Therefore, it is clear that the dynamic fluctuation and enhanced coarsening kinetics of Au NPs come from building up of charge. Again, it can be said that the enhanced coalescence kinetics previously observed directly by in-situ TEM (*15*) and

implied indirectly in the growth of nanowires and films by charged NPs comes from the charge.

Fig. 35-36 is that statistical analysis shows the number density and nearest neighbor distance, respectively. Fig. 35 (a) and Fig. 36 (a), the materials in the floating system show the same decrease and increase regardless of the conductivity. As shown in Fig. 35 (b) and Fig. 36 (b), in the ground system, SiO has a sharp gradient as in the case of floating, while there is little variation in graphene. The meaning of this data is that when the nanoparticles grow, they catch and grow nearby particles, and the time difference can be confirmed by statistical processing according to the time, growth can be accelerated by charge in a view of 'Non-classical crystallization'

A special point in this experiment is that the reacted region and the size of the irradiated electron beam are precisely the same, which means that a specific reaction in the reaction region has affected coalescence. This means that the influence of temperature on the reaction can be excluded once again. Since the particles having a flux have a gradient, if the temperature has worked, a change outside the probe size region must also have occurred. (Fig 37)

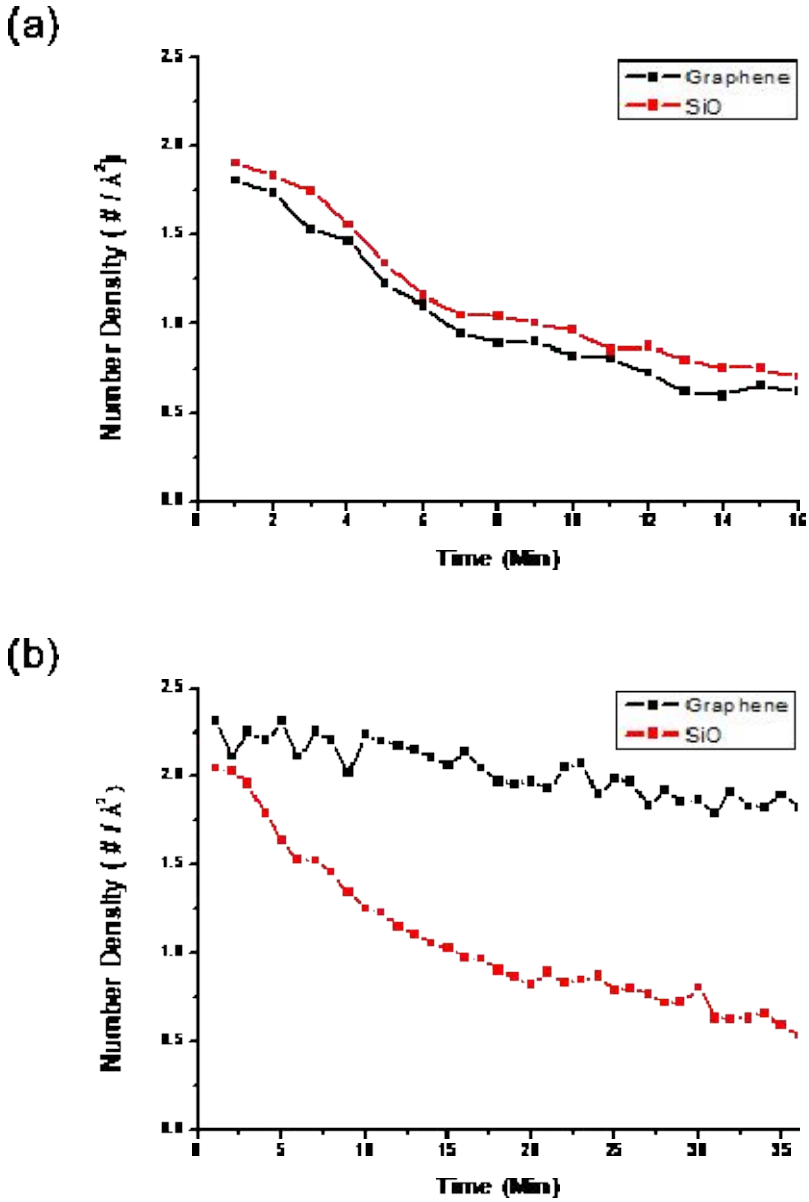

Figure 35 Variation in number of density over time (a) Floating (b) Ground

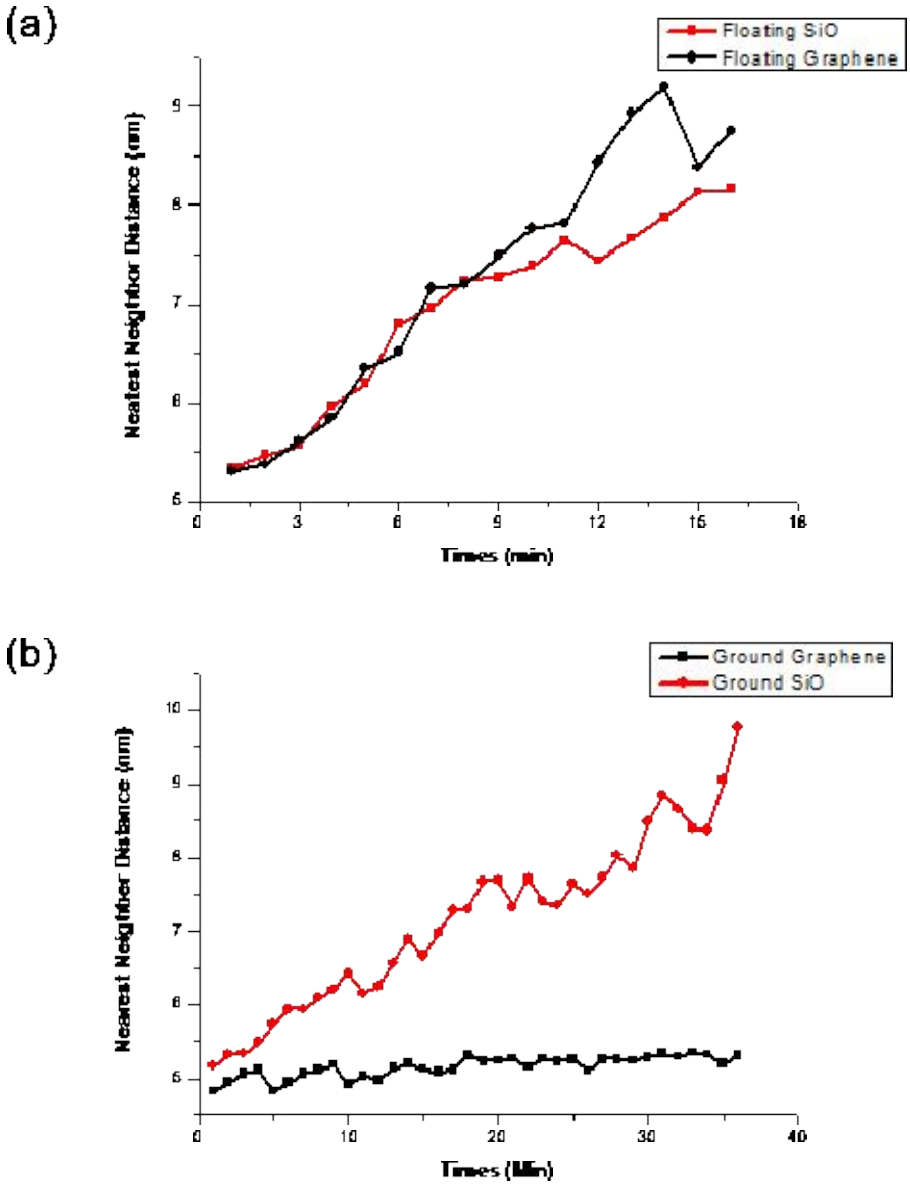

Figure 36 Variation of nearest neighbor distance over time (a) Floating (b) Ground

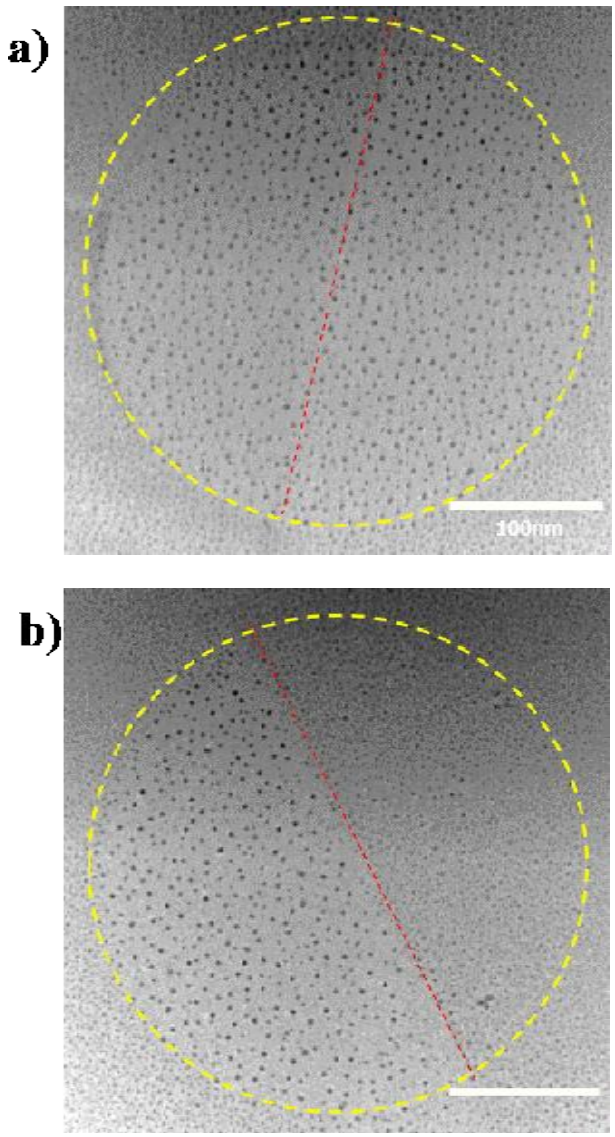

Figure 37 Evolution of nanoparticles in the region of interest (a) Floating (b) Ground

4.4 Behavior of Ag Nanoparticles in Floating & Ground systems

Although the theory of charged nanoparticles can be limited to 'charge' through previous experiments, there is a limit to the generalization in experiments using Au nanoparticles. There are a variety of approaches for generalization, but the first thing to do is whether the same mechanism can be adapted in materials with similar properties. Ag has been chosen in this respect as a suitable material that can replace gold and that the same deposition method can be used. Like the previous experiment, the same floating and ground system was implemented using a sputter. (Fig. 38) Fig 38 (a) and (b) show the floating system, and (c) and (d) show the ground system. As in Au experiments, floating systems have slightly different initial nanoparticle sizes, but both floating and ground have the same final configuration. However, if there is a peculiar point, the coalescence speed is confirmed to be less than 1 second when there is a charge in the Au nanoparticle experiment, but in the case of silver, if the measured video is not reproduced at a slow rate, it is difficult to confirm whether the same mechanism worked in Ag system. In the early analysis, the interpretation of this experiment was comprehended as melting and sublimation, but through precise analysis, it was confirmed that coalescence occurs at the moment. Unfortunately, this part could not be extracted as an image, so I could not put it in this thesis.

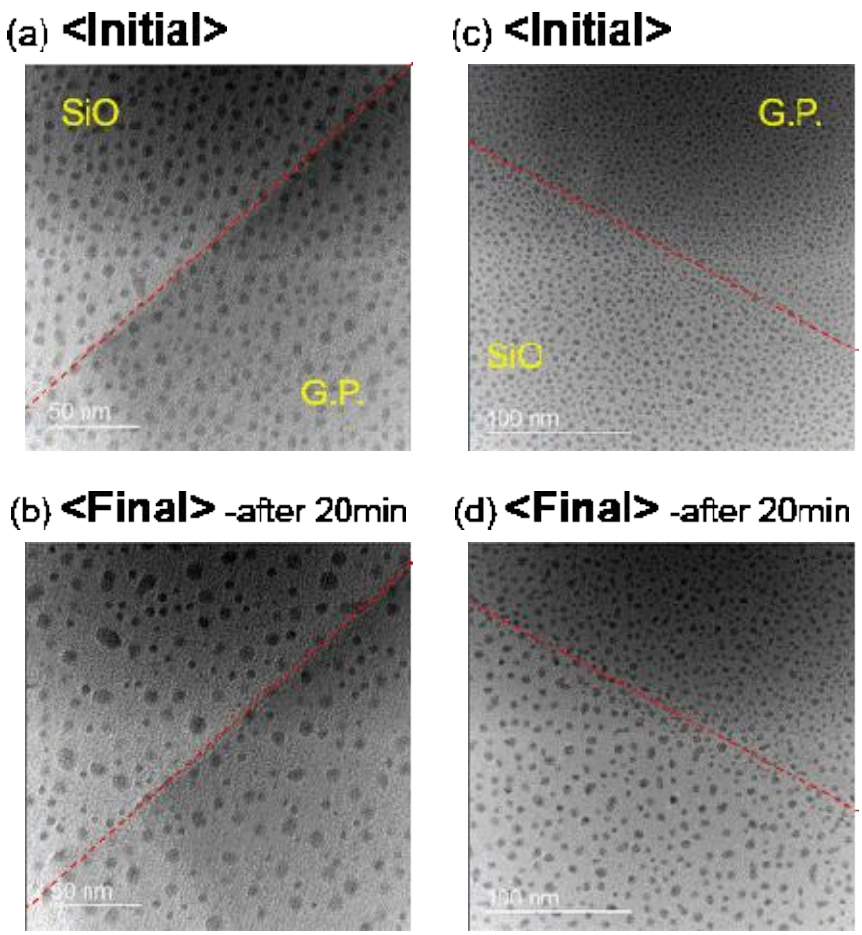

Figure 38 (a)-(d) show the time evolution TEM images of Ag NPs on the floating and ground system during 20 min. (a) and (b) represent the floating system, (c) and (d) represent the ground system.

4.5 Conclusion

Real-time observation in the TEM has potential for various controversies due to electron beams with high energy. To solve this problem, we implemented 1) an artificial charging system using the same material 2) It was placed on a grid so that it could be observed under the same TEM condition. It was confirmed that the charging behavior clearly improves the behavior of the particles by confirming the clear difference of the behavior of the particles according to the conditions that the charged particles escape and the particles do not go out even though the same material is used.

Ch.5 Summary

I have studied the difference of the behavior of the nanoparticles according to the conductivity of the substrate through in-situ TEM observation. We found that structural transformation of one nanoparticle and coalescence phenomenon between two particles were confirmed by the kinetic analysis according to the presence of charge, which enhances atomic diffusion. Furthermore, we realized an artificial charging systems on the same material, we confirmed only the effect of charge except for the other factors.

Chapter 2. The basic element for understanding non-classical particle growth as a theory of charged nanoparticles is to artificially create and observe one charged particle. Inelastic scattering between the electrons and the sample, which have high energies in the TEM, provides an environment in which nanoparticles can become charged. In this experiment, one particle was observed by controlling the artificial charge environment according to the conductivity of the substrate. The charged particles with charged charges are unstable due to a change in crystal structure or shape in real time, or even separated from the substrate. On the other hand, the uncharged collector shows that the crystal structure does not change despite the long time. This is due to the liquid-like nature of the charged nanoparticles, as the additional electrostatic energy from charge is injected and the energy of the whole system is increased.

Chapter 3. The energy of nanoparticles is very unstable due to the external factors that stimulate it because the ratio of surface energy is very high. This increase in energy due to external stimuli causes coalescence phenomenon when multiple particles are present. In this experiment, coalescence of two or more nanoparticles was analyzed dynamically according to the conductivity of the substrate. The time difference of about 15 times according to the change of the substrate depending on the charged state indicates that the electrostatic energy presented when observing the above one nanoparticle was involved in the total energy. In the coalescence of all grains, it was confirmed that oriented attachment, which is a characteristic of non-classical grain growth method, is common. The correlation of similar coalescence time on several substrates is related to the electrical resistance rather than the environment of the substrate, suggesting that charge can have a significant effect on coalescence kinetic.

Chapter 4. real-time observation in the TEM has potential for various controversies due to electron beams with high energy. To solve this problem, we implemented 1) an artificial charging system using the same material 2) It was placed on a grid so that it could be observed under the same TEM condition. It was confirmed that the charging behavior clearly improves the behavior of the particles by confirming the clear difference of the behavior of the particles according to the conditions that the charged particles escape and the particles do not go out even though the same material is used.

I have confirmed that the effect of charge is confined to nanoparticles and

that this can affect kinetic aspects in forming nanostructures through the preceding series of steps. I think that the enhanced kinetics by charge is a newly discovered phenomenon, which can open new science, technology and applications.

Reference

1. S. Moon, S. Tanaka, T. Sekino, Crystal growth of thiol-stabilized gold nanoparticles by heat-induced coalescence. *Nanoscale Res Lett* **5**, 813-817 (2010).
2. S. B. Simonsen *et al.*, Direct observations of oxygen-induced platinum nanoparticle ripening studied by in situ TEM. *J Am Chem Soc* **132**, 7968-7975 (2010).
3. J. F. Banfield, S. A. Welch, H. Zhang, T. T. Ebert, R. L. Penn, Aggregation-based crystal growth and microstructure development in natural iron oxyhydroxide biomineralization products. *Science* **289**, 751-754 (2000).
4. L. M. Qi, H. Colfen, M. Antonietti, Crystal design of barium sulfate using double-hydrophilic block copolymers. *Angew Chem Int Edit* **39**, 604-+ (2000).
5. E. R. Leite *et al.*, Crystal growth in colloidal tin oxide nanocrystals induced by coalescence at room temperature. *Applied Physics Letters* **83**, 1566-1568 (2003).
6. Z. Zhang *et al.*, Three-Dimensionally Oriented Aggregation of a Few Hundred Nanoparticles into Monocrystalline Architectures. *Advanced Materials* **17**, 42-47 (2005).
7. D. Gebauer, A. Volkel, H. Colfen, Stable prenucleation calcium carbonate clusters. *Science* **322**, 1819-1822 (2008).
8. R. Demichelis, P. Raiteri, J. D. Gale, D. Quigley, D. Gebauer, Stable prenucleation mineral clusters are liquid-like ionic polymers. *Nat Commun* **2**, 590 (2011).
9. H. H. Teng, How Ions and Molecules Organize to Form Crystals. *Elements* **9**, 189-194 (2013).
10. H. Colfen, S. Mann, Higher-order organization by mesoscale self-assembly and transformation of hybrid nanostructures. *Angew Chem Int Ed Engl* **42**, 2350-2365 (2003).

11. R. L. Penn, J. F. Banfield, Imperfect oriented attachment: dislocation generation in defect-free nanocrystals. *Science* **281**, 969-971 (1998).
12. Q. Zhang, S.-J. Liu, S.-H. Yu, Recent advances in oriented attachment growth and synthesis of functional materials: concept, evidence, mechanism, and future. *J. Mater. Chem.* **19**, 191-207 (2009).
13. S. Wohlrab, N. Pinna, M. Antonietti, H. Colfen, Polymer-induced alignment of DL-alanine nanocrystals to crystalline mesostructures. *Chemistry* **11**, 2903-2913 (2005).
14. H. G. Liao, L. Cui, S. Whitelam, H. Zheng, Real-time imaging of Pt3Fe nanorod growth in solution. *Science* **336**, 1011-1014 (2012).
15. J. M. Yuk *et al*., High-resolution EM of colloidal nanocrystal growth using graphene liquid cells. *Science* **336**, 61-64 (2012).
16. N. M. Hwang, J. H. Hahn, D. Y. Yoon, Charged cluster model in the low pressure synthesis of diamond. *Journal of Crystal Growth* **162**, 55-68 (1996).
17. N. M. Hwang, D. Y. Yoon, Thermodynamic approach to the paradox of diamond formation with simultaneous graphite etching in the low pressure synthesis of diamond. *Journal of Crystal Growth* **160**, 98-103 (1996).
18. N. M. Hwang, J. H. Hahn, D. Y. Yoon, Chemical potential of carbon in the low pressure synthesis of diamond. *Journal of Crystal Growth* **160**, 87-97 (1996).
19. N. M. Hwang, D. Y. Kim, Charged clusters in thin film growth. *International Materials Reviews* **49**, 171-190 (2004).
20. H. O. Pierson, *Handbook of Chemical Vapor Deposition (CVD) (Second Edition)*. (Noyes Publications, New York, 1992).
21. J. M. Huh, D. Y. Yoon, D. Y. Kim, N. M. Hwang, Effect of substrate materials in the low-pressure synthesis of diamond: approach by theory of charged clusters. *Z Metallkd* **96**, 225-232 (2005).
22. C. S. Kim, Y. B. Chung, W. K. Youn, N. M. Hwang, Generation of charged nanoparticles during the synthesis of carbon nanotubes by chemical

vapor deposition. *Carbon* **47**, 2511-2518 (2009).

23. C. S. Kim, W. K. Youn, N. M. Hwang, Generation of charged nanoparticles and their deposition during the synthesis of silicon thin films by chemical vapor deposition. *Journal of Applied Physics* **108**, (2010).
24. C. S. Kim, W. K. Youn, D. K. Lee, K. S. Seol, N. M. Hwang, Low-temperature deposition of crystalline silicon nitride nanoparticles by hot-wire chemical vapor deposition. *Journal of Crystal Growth* **311**, 3938-3942 (2009).
25. C. S. Kim, Y. B. Chung, W. K. Youn, N. M. Hwang, Generation of Charged Nanoparticles during Synthesis of ZnO Nanowires by Carbothermal Reduction. *Aerosol Science and Technology* **43**, 120-125 (2009).
26. S. S. Lee, C. S. Kim, N. M. Hwang, Generation of Charged Nanoparticles during the Synthesis of GaN Nanostructures by Atmospheric-Pressure Chemical Vapor Deposition. *Aerosol Science and Technology* **46**, 1100-1108 (2012).
27. Bockris, J. OM, Reddy, *Modern electrochemistry: An introduction to an interdisciplinary area*. (Plenum Press, New York, 1977).
28. R. F. Egerton, P. Li, M. Malac, Radiation damage in the TEM and SEM. *Micron* **35**, 399-409 (2004).
29. J. Su, X. Zhu, Atom Diffusion and Evaporation of Free-Ended Amorphous SiOx Nanowires: Nanocurvature Effect and Beam-Induced Athermal Activation Effect. *Nanoscale Res Lett* **11**, 514 (2016).
30. E. R. White, M. Mecklenburg, B. Shevitski, S. B. Singer, B. C. Regan, Charged nanoparticle dynamics in water induced by scanning transmission electron microscopy. *Langmuir* **28**, 3695-3698 (2012).
31. J. Cazaux, Correlations between Ionization Radiation-Damage and Charging Effects in Transmission Electron-Microscopy. *Ultramicroscopy* **60**, 411-425 (1995).
32. H. Suzuki, Z. Akase, K. Niitsu, T. Tanigaki, D. Shindo, Secondary electron effect on electron beam induced charging of SiO2 particle analyzed by electron holography. *Microscopy (Oxf)* **66**, 167-171 (2017).

33. S. Ino, Stability of Multiply-twinned particles. *Journal of the physical society of japan* **27**, 941 (1969).
34. S. Ino, S. Ogawa, Multiply Twinned Particles at Earlier Stages of Gold Film Formation on Alkalihalide Crystals. *Journal of the Physical Society of Japan* **22**, 1365-& (1967).
35. L. R. Wallenberg, J. O. Bovin, A. K. Petfordlong, D. J. Smith, Atomic-Resolution Study of Structural Rearrangements in Small Platinum Crystals. *Ultramicroscopy* **20**, 71-75 (1986).
36. T. Ben-David, Correlated Orientations in Nanocrystal Fluctuations. *Phys Rev Lett* **78**, 2585 (1997).
37. A. Stella, A. Migliori, P. Cheyssac, R. Kofman, Spontaneous Phase Fluctuations of Nanoparticles of Lead in a Silicon-Oxide Matrix. *Europhysics Letters* **26**, 265-270 (1994).
38. F. Baletto, R. Ferrando, Structural properties of nanoclusters: Energetic, thermodynamic, and kinetic effects. *Reviews of Modern Physics* **77**, 371-423 (2005).
39. M. J. Yacamán, J. A. Ascencio, H. B. Liu, J. Gardea-Torresdey, Structure shape and stability of nanometric sized particles. *Journal of Vacuum Science & Technology B: Microelectronics and Nanometer Structures* **19**, (2001).
40. S. Iijima, T. Ichihashi, Motion of Surface Atoms on Small Gold Particles Revealed by Hrem with Real-Time Vtr System. *Jpn J Appl Phys 2* **24**, L125-L128 (1985).
41. S. Iijima, T. Ichihashi, Structural instability of ultrafine particles of metals. *Phys Rev Lett* **56**, 616-619 (1986).
42. L. D. Marks, Experimental Studies of Small-Particle Structures. *Reports on Progress in Physics* **57**, 603-649 (1994).
43. E. Blaisten-Brojas, Melting and freezing of Lennard-Jones clusters on a surface. *Physical review B* **36**, 8447 (1987).
44. J. B. Wagner, M. G. Willinger, J. O. Muller, D. S. Su, R. Schlogl, Surface-charge-induced reversible phase transitions of Bi nanoparticles. *Small* **2**,

230-234 (2006).

45. A. Howie, Coulomb explosions in metals? *Nature* **320**, 684 (1986).
46. M. A. Asoro, D. Kovar, Y. Shao-Horn, L. F. Allard, P. J. Ferreira, Coalescence and sintering of Pt nanoparticles: in situ observation by aberration-corrected HAADF STEM. *Nanotechnology* **21**, 025701 (2010).
47. A. Courty, A. I. Henry, N. Goubet, M. P. Pileni, Large triangular single crystals formed by mild annealing of self-organized silver nanocrystals. *Nat Mater* **6**, 900-907 (2007).
48. N. Satoh, H. Hasegawa, K. Tsujii, K. Kimura, Photoinduced Coagulation of Au Nanocolloids. *The Journal of Physical Chemistry* **98**, 2143-2147 (1994).
49. R. Jin *et al.*, Photoinduced conversion of silver nanospheres to nanoprisms. *Science* **294**, 1901-1903 (2001).
50. H. G. Liao, H. Zheng, Liquid cell transmission electron microscopy study of platinum iron nanocrystal growth and shape evolution. *J Am Chem Soc* **135**, 5038-5043 (2013).
51. M. Giersig, I. Pastoriza-Santos, L. M. Liz-Marzán, Evidence of an aggregative mechanism during the formation of silver nanowires in N,N-dimethylformamide. *J. Mater. Chem.* **14**, 607-610 (2004).
52. M. A. v. Huis, L. T. K. Overgaag, Q. Xu, G. Pandraud, H. W. Zandbergen, Low-Temperature Nanocrystal Unification through Rotations and Relaxations Probed by in Situ Transmission Electron Microscopy. *Nano Letters* **8**, 3959-3969 (2008).
53. G. Boisvert, L. J. Lewis, M. J. Puska, R. M. Nieminen, Energetics of diffusion on the (100) and (111) surfaces of Ag, Au, and Ir from first principles. *Physical Review B* **52**, 9078-9085 (1995).
54. S. Iijima, P. M. Ajayan, Substrate and Size Effects on the Coalescence of Small Particles. *Journal of Applied Physics* **70**, 5138-5140 (1991).
55. K. S. Novoselov *et al.*, Electric field effect in atomically thin carbon films. *Science* **306**, 666-669 (2004).
56. F. Huang, H. Z. Zhang, J. F. Banfield, Two-stage crystal-growth kinetics

observed during hydrothermal coarsening of nanocrystalline ZnS. *Nano Letters* **3**, 373-378 (2003).

57. W. Neng, L. Shuang-ying, X. Jun, M. Martini, A 'jump-to-coalescence' mechanism during nanoparticle growth revealed by in situ aberration-corrected transmission electron microscopy observations. *Nanotechnology* **27**, 205605 (2016).
58. H. Li, X. C. Zeng, Wetting and interfacial properties of water nanodroplets in contact with graphene and monolayer boron-nitride sheets. *ACS Nano* **6**, 2401-2409 (2012).
59. W.-K. Youn *et al.*, Comparison of the Deposition Behavior of Charged Silicon Nanoparticles between Floating and Grounded Substrates. *The Journal of Physical Chemistry C* **118**, 11946-11953 (2014).
60. K. Choi, S. J. L. Kang, H. M. Jang, N. M. Hwang, Nucleation behavior in the presence of charge in the CVD diamond process. *Journal of Crystal Growth* **172**, 416-425 (1997).

국문 초록

나노 구조체의 형성은 고전적으로 원자나 이온, 분자에 의한 소립자의 적층으로 성장한다는 것이 일반적인 메커니즘으로 받아들여져 왔다. 다양한 분야의 나노 구조체의 응용이 가능하게 된 오늘날 다양한 연구에서 고전적인 성장 메커니즘으로 설명할 수 없는 기하학적인 구조들이 생성 또는 합성이 되고 있다. 이는 '비 고전적 결정 성장 (Non-classical Crystallization)'로 명명 되는 새로운 학문 분야로서 나노 구조체의 조합이 나노 입자 단위로 생성된다는 새로운 접근 방법을 제공한다.

이 새로운 학문 분야의 정립은 대부분 액상에서 합성된 물질을 관찰 및 보고를 통하여 되고 있으나, 일찍이 본 실험실에서는 액상 뿐만 아니라 기상에서 또한 이 현상이 일어남을 간접적으로 증명해왔다. 다만, 이를 해석하는데 있어서 독창적으로 적용되는 것이 '하전'에 대한 효과로, 기상에서 생성되는 나노 입자가 하전을 가질 때 'Liquid-like'한 성질을 가져 이것이 나노 구조체를 형성하는 기본 단위가 된다는 것이 핵심이고, 이것을 '하전된 나노 입자 이론(Theory of Charged Nanoparticle)'로 명명해왔다.

앞선 비 고전적 결정 성장방법에 대한 메커니즘은 아직 명확하게 정립되지 않는 영역으로, 다만, 중간 단계는 'Oriented attachment'가 일어나는 것은 잘 알려져 있다. 이런 나노입자에 의한 성장의 주도니 원동력은 표면 에너지의 감소를 위한 것으로 이를 예측하기 위한 다양한 모델들이 제시되고 있다. 이에 맞춰 제공되는 핵심 증거는 직접적인 육안 관찰이 가능한 투과전자현미경(TEM)을 이용한 실시간 관찰을 통하여 다양한 주장들이 제기되고 있다. 논의 되고 있는 다양한

메커니즘 속에서 투과전자현미경을 사용했을 때에 높은 에너지를 가지는 가속된 전자에 의한 타켓 물질과의 상호 작용에서 발생할 수 있는 하전의 영향을 간과하고 있는바, 본 학위논문에서는 하전에 초점을 두고 이것이 시스템 내에 존재했을 때 나노 구조체에 어떠한 영향을 미치는지에 대해서 체계적인 실험을 진행하였다.

일차적으로 타켓으로 삼은 금 입자를 기판의 전도성에 따라 입자의 거동 차이를 확인하였다. 인위적으로 하전을 띠고 있는 비 전도성 기판 위에서의 금 입자는 매우 불안정한 거동을 띠고 있음을 확인하였으나 대조군인 전도성 기판에서는 긴 시간동안에도 안정적인 형태를 띰을 확인하였다. 이에 더해, 비 전도성 기판 위의 금 입자가 기판에서 탈락됨을 통하여 척력, 즉 정전기적 반발력이 입자와 기판 사이에 작용하는 것이 관찰됨에 따라 시스템 내 입자에 하전을 인위적으로 구현할 수 있었다.

이에 더 나아가 하전 유무에 따른 나노 입자들간의 상관관계를 2개 이상의 입자가 존재하였을 때 관찰하였다. 나노 입자의 표면 에너지를 줄이기 위한 방법 중 하나인 coalescence가 일어나는 시스템 내에서, 하전이 존재할 때 약 15배 정도의 시간적인 빠르기를 가지고 이 메커니즘이 작용함을 확인함에 따라 나노 구조체를 형성하는데 있어서 하전은 나노 입자의 불안정성을 야기 시킴과 동시에 동역학적인 장벽을 낮추는 효과까지 가짐을 확인하였다.

마지막으로 이러한 관찰을 TEM을 이용하여 진행할 때에 제기될 수 있는 온도 상승, Hydrocarbon 오염, 다양한 기판을 사용함에 따른 타켓 물질이 처한 환경적 차이에 따른 논란을 해결하는데 중점을 두었다. 온도 상승은 관찰하는 환경의 전체적인 온도를 액체 질소 온도 까지 내림으로서 활성 장벽을 높였음에도 불구하고 coalescence가 일어나 이것에 대한 온도 영향을 배제하려고 하였고, 전도성과 비전도성 물질의

관찰간 발생하는 시간적인 간극에 따른 TEM의 환경과 샘플의 변화를 배제 하기 위하여 이를 하나의 TEM Grid 위에 하전이 존재할 수 있는 환경과 존재할 수 없는 환경을 한 번에 구현함으로서 해결하고자 하였다. 동일한 물질을 사용한 Floating & Ground 시스템은 명확하게 하전만 변수로 삼을 수 있는 환경을 제공하였으며, 관찰 전 후의 명확한 차이를 통하여 나노 구조체를 형성하는 환경 내에서 하전이 중요변수로 작용할 수 있음을 보였다. 또한, 이를 은 입자에 적용함으로서 금 입자로 구성된 앞의 실험을 넘어 하전 효과를 다른 물질로 적용하여 일반화 시킬 수 있는 작은 단서를 같이 제공하였다.

주요어 : 비고전적 입자성장, 하전된 나노입자, 금속 입자(금, 은), 기판 전도성, 실시간 투과전자 현미경, 인위적 하전 시스템

학 번 : 2012-30916

이 름 : 김 근 수